Chapter 6
The Issue of Solid-Solid Contact in Catalytic Soot Oxidation and the Benefits of Catalyst Nanostructuring to Regeneration of Catalytic Diesel Particulate Filters

Gianluca Landi, Valeria Di Sarli, Almerinda Di Benedetto, and Luciana Lisi

6.1 Introduction

Diesel particulate filters (DPFs) represent the best option for removing particulate matter (PM), which is mostly composed of carbonaceous particles called "soot," from diesel engine exhaust. A DPF is typically made of a ceramic material, such as cordierite or silicon carbide (SiC). It consists of thousands of square-section parallel channels, with the opposite ends of adjacent channels being plugged (Fig. 6.1).

Figure 6.2 shows a schematic representation of the flow path in a channel of a "wall-flow" DPF.

The exhaust gas enters the inlet channel and passes through the porous walls to the adjacent outlet channels. This "wall-flow" path allows the soot particles to be retained in the inlet channels. More specifically, soot is accumulated inside the filter according to two distinct mechanisms of filtration [1]. The soot particles are first trapped inside the porous walls of the filter according to the mechanism of "deep-bed filtration." When the maximum packing density is reached, the walls become substantially impermeable to the particles, and a soot layer, also called "cake," is built up onto the porous filter surface. The formation of the cake layer is an important advantage for the filtration performance, given that the cake itself acts as a filter [1]. Indeed, most of the soot accumulated inside a DPF is trapped under this form, i.e., according to the mechanism of "cake filtration."

G. Landi · V. Di Sarli (✉) · L. Lisi
Istituto di Scienze e Tecnologie per l'Energia e la Mobilità Sostenibili (STEMS), Consiglio Nazionale delle Ricerche (CNR), Naples, Italy
e-mail: valeria.disarli@cnr.it

A. Di Benedetto
Dipartimento di Ingegneria Chimica, dei Materiali e della Produzione Industriale, Università di Napoli Federico II, Naples, Italy

M. Piumetti, S. Bensaid (eds.), *Nanostructured Catalysts for Environmental Applications*, https://doi.org/10.1007/978-3-030-58934-9_6

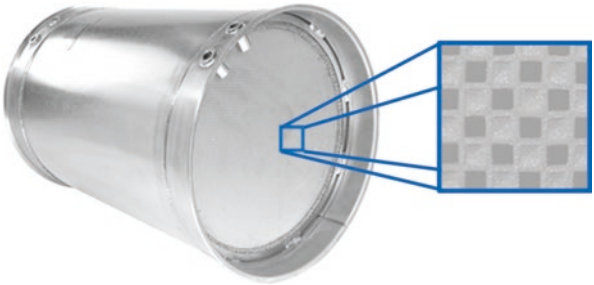

Fig. 6.1 A diesel particulate filter (DPF)—the magnified image shows the alternatively open and closed channels

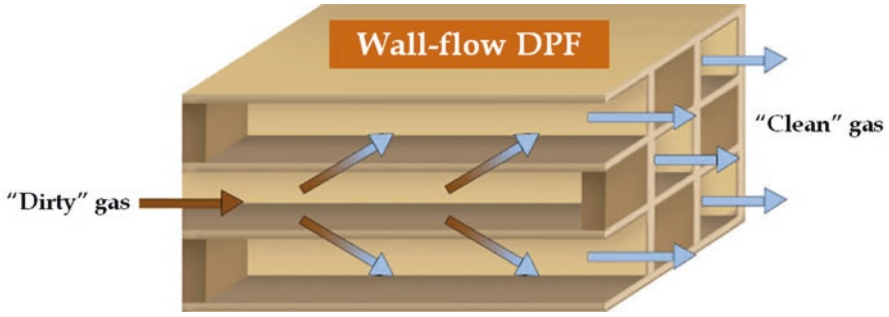

Fig. 6.2 Schematic representation of the flow path in a channel of a "wall-flow" DPF

The collected soot increases the backpressure of the diesel engine reducing its efficiency. Thus, the DPF needs to be periodically regenerated (cleaned) by soot combustion. Unfortunately, the temperature of the diesel exhaust gas (200–350 °C) is much lower than the temperature required to initiate and maintain soot oxidation. To raise the temperature up to the point that soot oxidation can be self-sustained in the filter at fast enough rates (>600 °C), external or engine (i.e., active) means (e.g., fuel burners, electric or microwave heating, injection of fuel in the exhaust, recirculation of exhaust gas, etc.) can be employed. Such an approach, also referred to as thermal regeneration, incurs additional energy costs and requires complex control techniques. Furthermore, in some cases, it can lead to the formation of excessively hot regions causing irreversible damage to the filter [2]. Finally, during thermal regeneration, soot is oxidized mostly to CO (values of selectivity to CO_2 around 40–50% were found [3, 4]).

Alternatively or complementarily, catalytic measures can be used to achieve soot oxidation at lower temperatures (250–550 °C) and/or to shorten the regeneration time period, thus allowing for energy saving (at an added cost of the catalyst).

Fuel-borne catalysts (FBCs), i.e., additives that are mixed with the fuel to lead to the formation of catalyst-doped soot during combustion in the engine, have been proposed as catalytic regeneration systems [5]. Additives are soluble compounds (octano-

ates, naphthenates, etc.) of metals (copper, iron, cerium, lead, manganese, etc.). In May 2000, PSA Peugeot Citroën launched the first series-production diesel passenger vehicle equipped with such a system. In particular, they used a Ce-based additive. By its sacrificial burning, particles of cerium oxide can be produced and embedded into soot particles, thus providing intimate soot-catalyst contact. This strategy has several critical issues. It requires the installation of a second tank for continuous additive supply in the fuel. The additive consumption leads to the accumulation of metal oxide "ash" inside the DPF, altering its structure. The fate of the catalyst particles after regeneration can be a further issue. Indeed, CeO_2 nanoparticles have a high long-term exposure toxicity [6]. To overcome these problems, the catalyst can be attached directly onto the walls of "catalytic" (i.e., catalyst-coated) DPFs.

Extensive research efforts have been focused on catalytic DPFs. However, there is still no general consensus regarding their ability to oxidize soot at low temperatures and under conditions relevant to practical applications. Indeed, catalytic soot oxidation involves a solid-solid catalysis, and thus, the regeneration performance of catalytic DPFs is dependent not only on the catalyst activity [3, 7], but also on the quality of the contact established between soot and catalyst particles [3, 4, 7–9]. As will be discussed in more detail in the following sections, in this framework, the development of effective catalytic DPFs is strictly linked to the development of nanostructured materials.

Nanoparticles are defined as particles having a diameter of less than 100 nm (0.1 μm) if spherical, while non-spherical nanoparticles are defined as particles with at least two dimensions smaller than 100 nm. When scaling down from micro to nano, physical, and chemical properties of particles significantly change both quantitatively and qualitatively. As expected, nanomaterials have a larger specific surface area than micromaterials. However, this is not the unique feature of nanoparticles with respect to microparticles. Nanoparticles exhibit significantly different properties with respect to microparticles, such as a greater reactivity, strength, fluorescence, conduction, etc. As a consequence, the scaling down from micro to nano does not trivially lead to an increase of catalyst activity related to a larger surface exposure, but it also changes the properties of the particles from an electronic point of view, thus changing their behavior and interaction with reactants and products. In other words, it also changes the intrinsic activity of the catalyst. For these reasons, nanoparticles are widely used in catalysis.

In heterogeneous catalysis, reaction occurs at the interface between the solid catalyst particle and reactants, which may be gaseous, liquid, and/or solid. The increase of the surface-to-volume ratio significantly affects the contact between reactants and active phase, thus enhancing the reactivity. But more importantly, it has been found that, when decreasing the particle size down to nanometers, the electronic state and the coordination environment of surface atoms undergo significant changes [10]. Goodman and coworkers [11] first demonstrated the role of nanosize in affecting the electronic character of Au nanoparticles supported on TiO_2 in CO oxidation. A gold nanoparticle at 1–2 nm may exhibit a molecule-like electronic state instead of a metallic state. This issue may strongly affect the catalytic performance.

Among all the catalysts investigated at the nanoscale, a prominent role is played by ceria. Several studies have shown that, due to the high surface area and highly reactive morphologies, ceria-based nanomaterials can be effectively used as catalysts for organic transformation reactions such as oxidation, reduction, hydrogenation, coupling reactions, and many more [12–14].

From the point of view of (nano)catalyst development and, more generally, chemical engineering, catalytic soot oxidation is a very interesting topic. Several issues are to be taken into consideration and linked to each other. First of all, solid-solid catalysis requires an intimate contact between reactant (soot) and active phase. The development of highly active catalysts is also a fundamental aspect requiring: (1) high mobility of oxygen and propensity to form surface active species; (2) nanostructure and/or special morphologies (in order to improve both contact and intrinsic activity); and (3) structural stability. In addition, there is a significant contribution of the interaction between solid phases and gaseous reactants to the catalytic performance, particularly in regard to the presence of gaseous oxygen carriers. Finally, engineering of particulate filters with nanostructured catalysts is not a trivial task. Most of these aspects are clearly related to each other, and thus, it is quite difficult to discuss each of them separately. In the following, we present sections devoted to specific topics and discuss the most relevant literature results in order to highlight how the issues mentioned above have been addressed and what solutions have been proposed. Obviously, the reader should consider that the topics of the different sections may partially overlap.

6.2 Type of Soot-Catalyst Contact

Soot typically consists of agglomerates with about 100 μm in size composed by smaller open particles in the range 0.1–1 μm, which in turn are made up of carbonaceous spherules of 10–50 nm (Fig. 6.3). The agglomerates can be easily disaggregated by treatment in ultrasound bath. The spherules are stuck together by shared carbon deposition forming the loose particles of 0.1–1 μm size. Although these particles have a high porosity (up to 0.95), they cannot be broken down into the individual spherules even by strong ultrasound treatment [15].

The surface of the spherules has adhering hydrocarbon material or soluble organic fraction (SOF) and inorganic material (mostly sulfates). Nevertheless, real soot collected from diesel engines under real conditions strongly depends on engine parameters, and consequently, Printex U is often used as model soot in studies reported in the literature [17].

The contact between the carbonaceous material and the grains of a solid catalyst is of paramount importance. Indeed, if the catalyst grains are not in intimate contact with the carbon surface, their effect will be lower. Ciambelli et al. [18] postulated two reactivity relationships, one for spherules within the field of action of the catalyst and another one for those initially outside. At lab-scale, Neeft et al. [19] developed two methods of mixing catalyst with soot, which they termed “loose” and

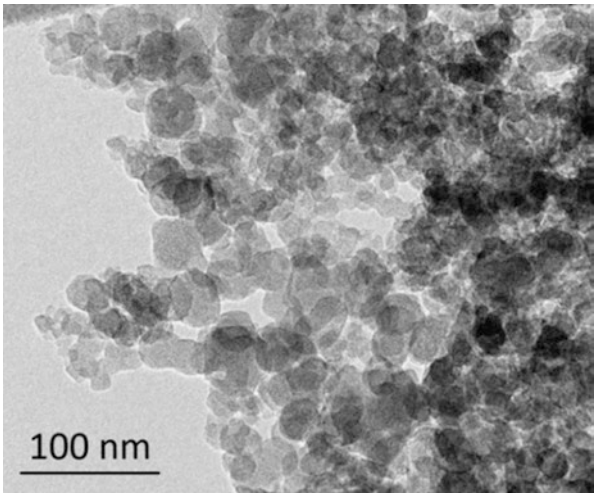

Fig. 6.3 Micrograph of typical diesel soot: particles consist of clusters of spherules [16]

"tight." The catalysts were prepared as particles of less than 125 μm size. In the loose mode, catalyst and carbon black (CB), with a 2:1 mass ratio of catalyst to CB, were simply mixed together with a spatula. In the tight mode, a mixture at the same ratio was mechanically milled for an hour. Since then, most of scientists who investigated new catalytic systems evaluated the catalytic performance using one or both types of contact between soot and catalyst particles, generally through temperature-programmed oxidation (TPO) experiments carried out in thermobalance consisting in an oxidation by increasing temperature of a soot-catalyst mixture.

The loose and tight methods allow a more reliable classification of the catalyst activity, although the catalytic performance can deeply depend on the contact type. Figure 6.4 shows the results obtained by Quiles-Díaz et al. [20] on a 2% CuO/ceria-zirconia catalyst and gives an example of the different behavior of the two contact systems.

Combustion of soot in tight contact with the catalyst takes place at significantly lower temperatures. Indeed, the tight mode forces soot and catalyst to be in intimate contact with each other. Generally, this analysis is used to discriminate catalysts in terms of intrinsic activity, because soot oxidation is not rate-limited by a poor soot-catalyst contact. On the other hand, the loose contact better reproduces the oxidation behavior of soot in the catalyzed (i.e., catalyst-coated) DPF.

Christensen et al. [21] evaluated the rate constant of various metal and metal oxide catalysts in loose and tight contact with soot. Regardless of the contact type, the rate constant outlines a volcano curve when plotted against the heat of oxygen chemisorption on the catalytic material. However, the maximum in the volcano curve corresponds to different values of heat of oxygen chemisorption for the two contact situations, and this result was attributed to mechanistic differences between oxidation in loose and tight contact. Among the tested catalysts, Co_3O_4 and CeO_2 are those closer to the maximum in tight contact, whereas Cr_2O_3 is closer to the maximum in loose contact. For both contacts, the activation energy for soot oxidation

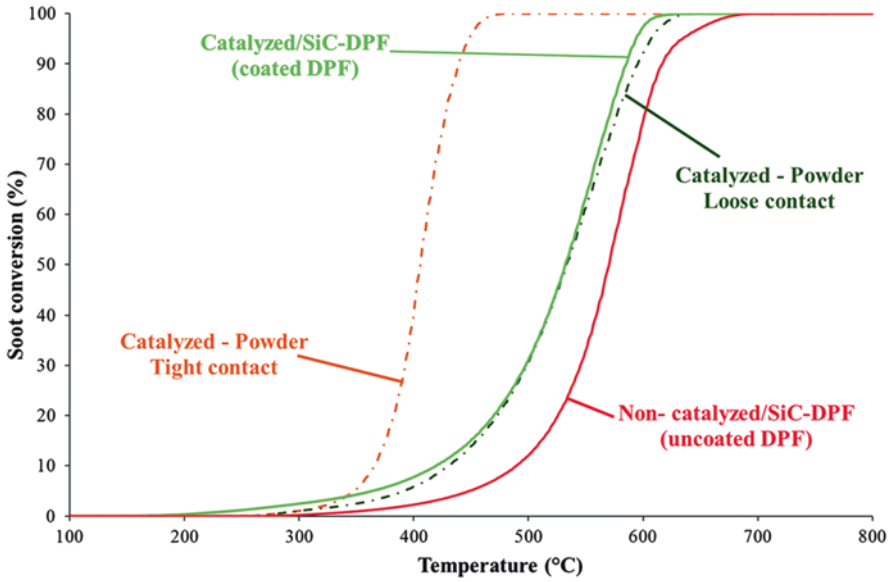

Fig. 6.4 Soot conversion curves versus temperature during heating-ramp experiments for different catalytic configurations [20]

follows a linear Brønsted-Evans-Polanyi relationship with the heat of oxygen chemisorption. However, the slope differs, being higher in loose contact. This suggests a transition state closer to the final state, namely a complete rupture of the oxygen-catalyst bond in loose contact.

Neeft et al. [19] found that the reaction rate is strongly influenced by the mass ratio of soot to catalyst, and the burn-off temperature significantly decreases as the ratio is decreased.

Liu et al. [22] reported that the difference between the temperature of ignition (T_{ig}) of soot combustion and that of the maximum (T_m) during TPO experiments can be taken as a measure of the nature of catalytic sites versus the number of contact points between these sites and soot. Low values of T_{ig} indicate the presence of very active sites which are capable of lowering the activation energy for soot oxidation. Therefore, T_{ig} reflects the nature of the active species regardless of the number of catalytic sites present. Once ignition takes place, the number of catalytic active sites in contact with soot becomes important, as it determines the further combustion rate. A marked difference between T_{ig} and T_m indicates a poor contact, while a small difference indicates a very good contact between soot and catalyst.

Besides the loose and tight contact, there exists another type of contact, the "pressure" contact. Hensgen and Stöwe [17] reproduced this contact type pressing a loose mixture of soot and (nano)ceria (with a 4:1 mass ratio of catalyst to soot) in a hydraulic press forming pellets that were subsequently crushed down to powder in a mortar. These authors compared the three types of contact (loose, tight, and pressure). They found that the T50 temperatures obtained with tight contact are much

lower than in commercial DPF. On the other hand, the T50 temperatures of the loose and pressure contacts are similar to the temperatures in the real DPF systems, but the problem of these contacts is that no automation is possible. For five samples in loose contact, a standard deviation of T50 equal to 23.1 °C was reported. To reach a better reproducibility, a further contact type was developed by stirring the soot with the catalyst in acetone for 6 h. With this contact type, a better reproducibility, with a standard deviation of T50 of only 3.7 °C, was reached. This contact was called "wet" contact.

Hensgen and Stöwe [17] also studied the influence of the soot type on the contact mode. In particular, they investigated three different types of soot (fullerene soot (FS), Printex U (PU), and Printex 90 (P90)) in combination with the four different contact modes (loose, tight, wet, and pressure). In each contact mode, the T50 values of the FS are lower than those of the PU and P90 soot. For the loose, tight, and wet contacts, there exists a fixed order of the T50 value: tight < loose < pressure. The wet contact has not a fixed position within this order. While with PU, the wet contact is between the tight contact and the loose contact, with P90 and FS, the T50 value is even lower than in the case of the tight contact. Overall, in view of the standard deviations of the characteristic temperatures, the wet and tight contacts show similar T50 values, but the former is more reproducible.

Aneggi et al. [23] showed that a "supertight" contact can be obtained when ball-milling CeO_2-ZrO_2 powders and carbon soot for several hours. High-resolution transmission electron microscopy (HRTEM) revealed that the high-energy milling has the effect of progressively dissolving the large three-dimensional soot clamps and distributing more or less uniformly the carbon over the catalyst by wetting the catalyst surface with an almost two-dimensional thin layer of carbon. This result was also confirmed by the increasing metal/carbon atomic ratio detected by X-ray photoelectron spectroscopy (XPS). Accordingly, the number of contact points is significantly increased and the soot oxidation rate at low temperatures is boosted (a T50 value of 265 °C was found with 8 h milling). More recently, oxidation of soot in supertight contact with CeO_2-ZrO_2 was investigated by in situ environmental HRTEM from room temperature up to 550 °C, showing that the exceptional oxidation activity is related to the mobility of catalyst nanoparticles within the carbon globules during their consumption [24].

The results discussed above highlight the importance of the solid-solid contact in catalytic soot oxidation. The nanosize of the catalyst particles surely plays a key role in promoting this contact.

Lab-scale reaction conditions, especially if powdered soot-catalyst mixtures in tight (or similar) contact are used, can be significantly far from conditions of a real process of regeneration of catalytic DPF, thus limiting the possibility of extrapolation beyond the explored parameter ranges. On the other hand, studies in tight contact provide insight into the reaction mechanism and into the features related to the intrinsic activity, thus giving precious indications on the catalyst characteristics to be engineered in order to obtain improved catalytic systems.

6.3 Cerium Oxide (CeO_2)

CeO_2 is the most explored catalyst for soot oxidation [16]. This is also due to the fact that it is widely used in automotive three-way catalysts (TWCs) owing to its function of storage and release of oxygen under cyclic oxidizing and reducing environments. As a consequence, a lot of studies on the effect of the solid-solid contact on soot oxidation are focused on this material.

Simonsen et al. [25] studied CeO_2-catalyzed soot oxidation at the nanoscale by means of environmental transmission electron microscopy (ETEM). They found that catalytic oxidation involves processes that are confined to the region of the soot (carbon black, CB)-CeO_2 interface. Moreover, motions of CB agglomerates toward the catalyst surface act to re-establish the solid-solid interface and, thus, the CB-ceria contacts remain constant in the course of the oxidation process. Figure 6.5 shows the time-lapsed series of ETEM images recorded during CB oxidation over ceria.

It can be seen that agglomerates of CB particles move toward CeO_2 and vanish, whereas agglomerates of CB particles do not protrude and move away from the edges of the catalyst particles.

At the nanoscale, ambient pressure X-ray photoelectron spectroscopy (APXPS) revealed that soot oxidation over ceria involves two co-operative routes [26]. One occurs at the ceria-soot interface due to the formation of oxygen vacancies (related to Ce^{3+}); the other one occurs at the soot surface due to the formation of active superoxide species derived from the reaction between molecular O_2 and oxygen vacancies (Fig. 6.6).

Bassou et al. [27] evaluated the amount of oxygen transferred from ceria to soot via the soot-catalyst contacts using an experimental microkinetic approach. Consistently with the fact that the soot-ceria contacts do not change during oxidation

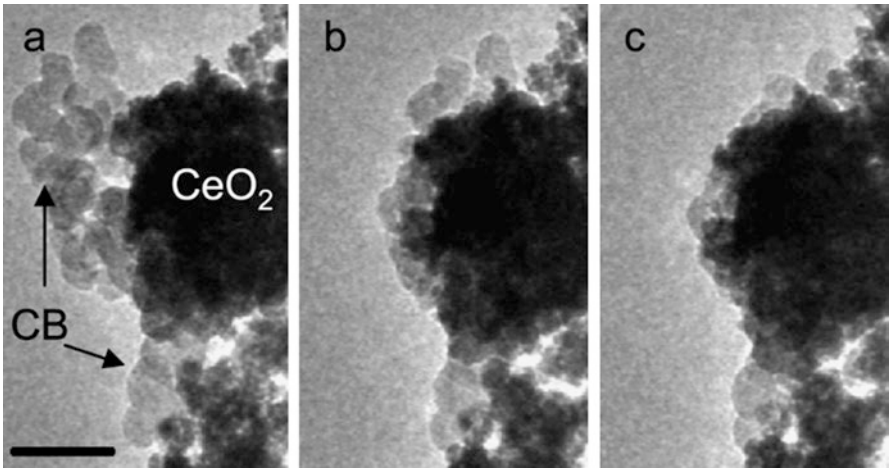

Fig. 6.5 Time-lapsed ETEM images during CB oxidation over ceria (the time interval between (**a**, **b**) images and (**b**, **c**) images is ~2 min; scale bar = 90 nm) [25]

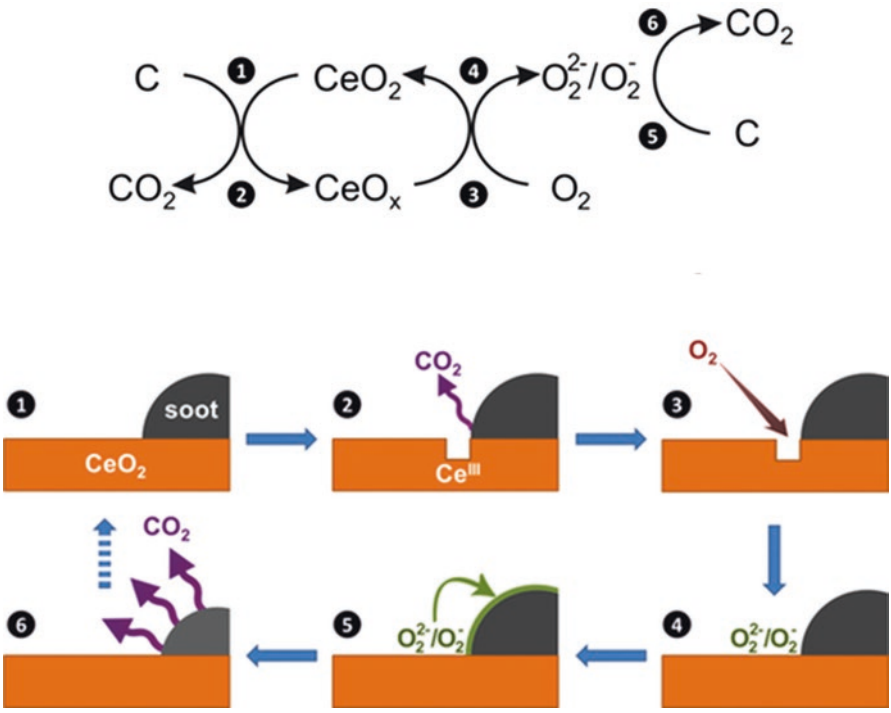

Fig. 6.6 The two co-operative routes involved in soot oxidation over ceria-based catalysts [26]

[25], they found that this amount (linked to the number of contacts) is constant with the progress of reaction, regardless of both type of soot-ceria contact (loose or tight) and ceria/soot weight ratio (10 or 1). This amount was evaluated after 2–3 cycles of temperature-programmed experiments with or without O_2, the first cycles being dominated by desorption and oxidation of the soluble organic fraction (SOF) preventing the evaluation of the oxygen transfer from ceria to soot from the productions of CO_2 and CO. However, the amount of oxygen available for soot oxidation (in μmol of O/g of soot) is dependent on the ceria-soot mixture and is correlated to the catalytic performance of ceria to decrease the temperature of soot oxidation by O_2. The authors also selected two plausible kinetic models (denoted as M1 and M2) of soot oxidation via surface defect sites, which are different by the implication (M2) or not (M1) of the diffusion of oxygen species on the ceria surface [28]. In the two models, the soot-ceria contacts are considered as a key kinetic parameter for soot oxidation. The active sites of soot (i.e., the carbon defect sites) and the active oxygen species of ceria are situated at the soot-ceria interface. The properties of this interface, such as the average number of contacts between a ceria particle and the soot particles, and the average surface area of a contact, are included in the mathematical formalism. The M1 model prevails at temperatures lower than 900 K, whereas the M2 model must be used at higher temperatures. This is due to the fact that surface oxygen species and, later, bulk oxygen species of ceria diffuse to the

interface, forming new active oxygen species. At high temperatures, it is the rate of diffusion of those species that controls the production of CO_2. The models were extended to soot oxidation in the presence of O_2. The M1 model provides theoretical curves consistent with experimental data, considering that rapid adsorption of oxygen on ceria allows for the surface concentration of active oxygen species to remain constant in the absence of external diffusion.

Issa et al. [29] developed a model for combustion of CB on the basis of experimental data obtained on mixtures of CB and a commercial CeO_2 with different CB/catalyst ratios and different contact conditions (loose and tight). The proposed model accounts for the size distribution of CeO_2 particles, the contact area between CB and CeO_2, the mass of CB in the sample, and the initial CB/CeO_2 ratio. It enables to satisfactorily predict the experimental combustion rate of CB.

Saab et al. [30] investigated the intensity of the soot-catalyst contact for mixtures of CB with CeO_2 (or Al_2O_3), in loose and tight contact, by means of electron paramagnetic resonance (EPR). The preliminary EPR analysis on CB showed a signal (S1) attributed to intrinsic paramagnetic centers on CB. Another signal (S2) was observed only with tight mixtures. The S2 signal was attributed to the formation of new paramagnetic species consistent with localized paramagnetic spins on the carbon particles and catalyst interface and, as such, was considered as a fingerprint of the contact between the two solids. It was found that these new paramagnetic species increase the reactivity of CB-CeO_2 mixtures in tight contact in the catalytic reaction of CB combustion.

The contact between soot (CB) and ceria was also investigated by SEM and EPR analyses [31]. Different procedures were followed to prepare loose and tight mixtures. CB, composed of primary particles in the 20–90 nm size range aggregated in structures with a foamy aspect, remains unchanged whatever the conditions of preparation of the mixture (mixing, grinding or sieving). CeO_2 alone is composed of aggregated grains in the 50–80 nm size range. Grinding CeO_2 samples provides particle disruption. SEM images showed a very limited solid-solid contact when CB and CeO_2 (with a 1:1 mass ratio) are ground together for 3 min (CeO_2 particles are sometimes surrounded by CB particles—loose sample), and an enhanced contact when CB and CeO_2 (at the same ratio) are ground together for 15 min (grinding promotes the formation of small catalyst particles and the increase of the contact points between the two solids—tight sample). In agreement with Saab et al. [30], the S2 EPR signal was identified as the paramagnetic print of the contact between CB and ceria. This signal was correlated to the number of soot-catalyst contact points, and the existence of a critical distance was suggested from which a liaison is established between the two solids communicating with each other through ultrathin gas bolster (with or without physical touch). When this liaison is not established or does not exist, the S1 signal is only identified. Conversely, when this liaison is established, both EPR signals are identified. The two signals were observed for both loose and tight samples. However, in the case of the loose sample, the S2 intensity is low compared to the S1 intensity confirming that the contact between CB and CeO_2 is very poor. In addition, the number of paramagnetic species of the S2 signal is much lower than that found with the tight sample.

6.4 Addition of Other Elements to Ceria

In order to improve the activity of ceria toward soot oxidation, the addition of other elements has been proposed [16].

Sudarsanam et al. [32] investigated CeO_2 nanocubes decorated with CuO_x nanoparticles. Higher concentrations of Ce^{3+} ions and abundant oxygen vacancies, especially at the (nano)interface between CuO_x and CeO_2, improve the performance toward soot oxidation with respect to pristine ceria in both loose and tight conditions. Cui et al. [33] found that the doping of Cu in CeO_2 nanoflakes significantly promotes the formation of oxygen species that replenish the vacancies in both tight contact and NO_x-assisted loose contact (the NO_x assistance will be discussed in Sect. 6.6). The highest activity was observed for the sample of $Cu_{0.2}Ce_{0.8}O_2$ nanoflakes and was attributed to its moderate doping that induces both a large amount of surface-adsorbed oxygen species and a special flake morphology, thus providing effective contact area. Sudarsanam et al. [34] reported that the addition of iron, but mostly of copper, to ceria nanorods increases the number of active oxygen species.

The addition of La to CeO_2 also generates higher amounts of active oxygen species at lower temperatures, which are effective for soot oxidation in tight contact, when the oxygen transport from catalyst to soot is not limited [35]. Nevertheless, in loose contact, the active oxygen transfer is difficult and, before reacting with soot, the active oxygen species recombine with each other to form O_2. In this situation, the increase in specific surface area induced by the addition of La is the only factor that affects the activity.

Lim et al. [36] "simulated" diesel particulate matter (PM), consisting of primary soot particles and soluble organic fraction (SOF) on the surface, by liquid-phase adsorption of SOF (eicosane, $C_{20}H_{42}$) on soot (carbon black). They used Ag, Pt and Pd supported on CeO_2 or TiO_2 as catalysts and tested PM oxidation in both tight and loose contact. The catalytic performance for oxidation of SOF and soot in simulated PM depends on both metal species and supports. CeO_2 has an inherent activity for both SOF and soot oxidation, while TiO_2 is nearly inactive for both reactions. For SOF oxidation, which is independent of the contact conditions, Pt is the most active metal followed by Pd and Ag. On the contrary, Ag is more active than Pt and Pd toward soot oxidation under both tight and loose contact conditions, this reaction taking place in tight contact at a temperature lower than in loose contact, as expected.

Neeft et al. [37] suggested that the catalyst mobility (ability to move into deposited soot) is a major parameter determining the activity in loose contact, and this mobility correlates with the melting point or the partial pressure of the catalyst. In particular, catalysts with a high mobility can be low-melting-point compounds, which can melt and wet the soot particles, or materials with a high vapor-phase mobility. Actually, the catalyst mobility is a required feature to reduce the difference in activity between tight contact and loose contact. From this point of view, the work by Gardini et al. [38] is very interesting. These authors investigated soot oxidation catalyzed by very active silver nanoparticles exhibiting a limited difference in activity between loose mode and tight mode. The dynamic evolution of catalytic

soot oxidation was visualized by means of in situ environmental transmission electron microscopy (ETEM) and bright-field TEM (BFTEM). The considerable activity of silver was at least in part ascribed to the significant mobility of the catalyst particles, responsible for ensuring the constant presence of a reactive soot-silver-oxygen interface. During soot oxidation, the reaction front moves, and attractive forces between metal and soot pull the silver particles along with the progressing front, thus causing a high mobility of the catalyst. The mobility is strongly influenced by the balance between attractive forces connecting silver agglomerates to the porous soot matrix and the size of the silver agglomerates themselves related to their internal cohesive energy. Figure 6.7 shows the BFTEM images of in situ oxidation of a soot-silver mixture in loose contact.

Mori et al. [39] investigated Ag/CeO_2-catalyzed soot oxidation at the nanoscale by means of ETEM. They found that reaction mainly occurs at the soot-catalyst interface (and not on soot itself), the soot particles gradually moving toward the catalyst and vanishing at the interface. They also observed that the silver-ceria interaction limits the formation of extremely large agglomerates of silver particles.

The addition of silver to ceria results in an enhanced soot oxidation activity with respect to pristine ceria [40–43]. Liu et al. [41] found that silver promotes the regeneration of O^-, present in large amount in spent CeO_2 catalysts, into highly active O_2^- leading to a ten-fold increase in soot oxidation activity over Ag/CeO_2 with respect to the unpromoted ceria catalysts. In agreement with these findings, Lee et al. [42] reported that the addition of silver to CeO_2 promotes the formation of the O_2^- superoxide, the amount of this active oxygen species being affected by the silver load. Zeng et al. [43] found that the presence of Ag nanoparticles induces a great number of oxygen vacancies in the CeO_2 lattice through the electronic transfer and that the Ag-assisted CeO_2 catalyst exhibits a better reduction performance. They also presented a reaction mechanism in which the O_2^- species is regarded as the determinant factor for the catalytic activity.

A positive effect of the silver addition was also reported by Deng et al. [44] for Ag/Ce-Zr catalysts. The catalysts were synthesized by precipitation in the presence

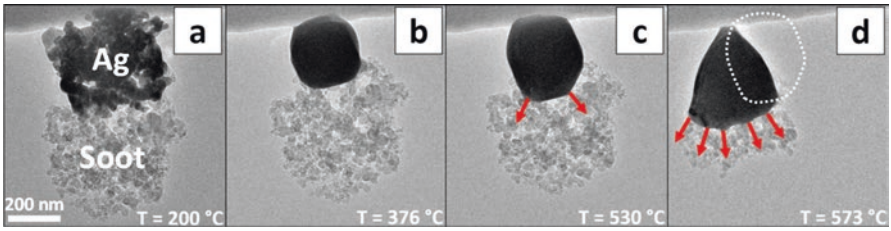

Fig. 6.7 Wetting and movement of a silver agglomerate during in situ oxidation of a soot-silver mixture in loose contact: BFTEM images showing (**a**) initial agglomeration and morphology of silver and soot, (**b**) coalescence of silver particles, (**c**) initial deformation of coalesced silver agglomerate due to capillary forces, and (**d**) movement of silver agglomerate. The red arrows indicate the direction of deformation of the silver agglomerate, and the dashed white line in sub-figure (**d**) highlights the previous position of the silver agglomerate as observed in sub-figure (**c**) [38]

of KOH and/or NH_3-H_2O, which allowed a good control of size and structure of the Ag particles. The very good performance in soot oxidation of the Ag-promoted catalysts, especially of those obtained using both precipitants, was attributed to the high capacity (associated with a suitable Ag^+/Ag^0 ratio) to activate and store oxygen species at a temperature much lower than unpromoted Ce-Zr. It was found that the high mobility of Ag contributes to the very good activity under loose contact conditions.

A good activity of Ag/CeO_2 was also reported by Corro et al. [45]. These authors did not use commercially available synthetic soot, but they generated soot by controlled combustion of several diesel-biodiesel blends. The addition of biodiesel to diesel modifies the soot composition, which becomes richer in aliphatic and oxygenated compounds. Thus, soot reacts faster over the Ag/CeO_2 catalyst (Fig. 6.8).

The addition of alkaline metals to CeO_2-based catalysts has also been proposed. Weng et al. [46] added potassium nitrate to copper-ceria catalysts. They found that the large amount of Cu-Ce interfacial sites is responsible for promoting the activation of oxygen, which is crucial for soot oxidation in tight contact. On the other hand, the low melting point of potassium nitrate improves the soot-catalyst contact in loose conditions. Alinezhadchamazketi et al. [47] found the same for K-added ceria-zirconia catalysts.

Sui et al. [48] prepared Cs-Ce-Zr catalysts by the sol-gel method. They reported that, under loose conditions, the solid-solid contact is improved and the soot oxidation rate speeds up when temperature is higher than that of melting of $CsNO_3$.

Shimokawa et al. [49] compared the addition of silver and potassium and found that K-promoted CeO_2 or TiO_2 samples oxidize catalytically a larger fraction of soot than Ag-promoted samples due to the higher mobility of K with respect to Ag in loose contact.

Zirconium has widely been used to partially substitute cerium forming mixed oxides. Ce-Zr mixed oxides have a higher specific surface area, a smaller crystal size, and enhanced redox properties, all features that determine a higher activity in

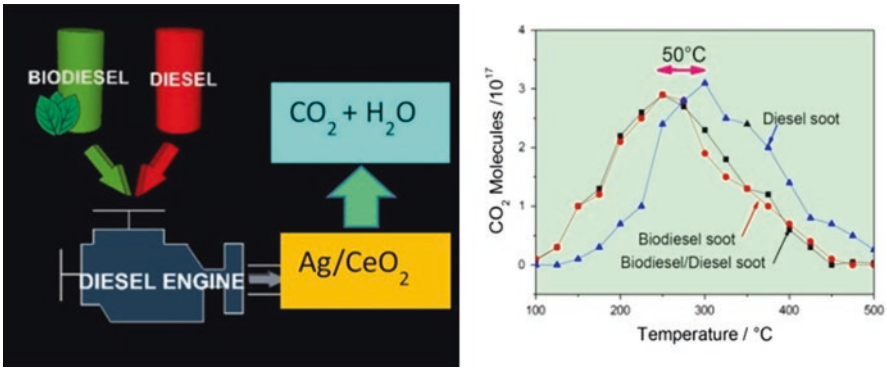

Fig. 6.8 The addition of biodiesel to diesel allows faster reaction of soot over Ag/CeO_2 catalyst [45]

both loose and tight contact. The substitution of Ce^{4+} for Zr^{4+} ions promotes the formation of defects (i.e., oxygen vacancies) in the ceria-zirconia lattice. Nevertheless, Piumetti et al. [50] showed that there exists a limit to the substitution of Ce^{4+} for Zr^{4+} because the surface density of the active redox element (Ce) decreases as the Zr content increases. They identified in $Ce_{0.9}Zr_{0.1}O_2$ the best composition of ceria-zirconia catalysts as nanopolyhedra. This morphology provides the best soot oxidation activity also compared to other catalysts with the same composition but different morphology, highlighting that the role of a suitable exposure of highly reactive planes prevails over the role of a large surface area.

Ce-Zr solid solutions were also studied by Trovarelli's group [23, 24, 26] with a focus on the soot-catalyst contact investigated at the nanoscale by means of advanced techniques, as already described in Sects. 6.2 and 6.3.

Trovarelli's group also investigated the activity of transition and alkaline-earth metal-doped catalysts supported on ceria or zirconia for NO_x-assisted soot oxidation [51]. A series of Cu- and Fe-impregnated catalysts over CeO_2 and ZrO_2 supports were prepared and characterized, and their catalytic activity was investigated by means of temperature-programmed oxidation (TPO) experiments. It was found that the copper-modified catalysts are more active. Moreover, the addition of Sr positively affects the performance of the materials, suggesting a synergic effect between transition metals and alkaline-earth metal. Copper is mainly involved in oxidation of NO to NO_2, which is a strong soot oxidizing agent, while strontium in the storage of NO_x species.

The role of copper as promoter of NO oxidation was also highlighted when this element was added to Ce-Pr solid solutions [52]. In particular, the benefit of mixing $Ce_{0.5}Pr_{0.5}O_{2-\delta}$ particles with and without copper in a single catalyst formulation was demonstrated. Indeed, the catalyst that combines $Ce_{0.5}Pr_{0.5}O_{2-\delta}$ particles with and without copper has two different types of active sites and optimizes the participation of two mechanisms of soot oxidation: the particles with copper mainly promote oxidation of NO to NO_2 (i.e., the NO_x-assisted mechanism), while those without copper are more effective in promoting the active oxygen mechanism.

In line with designing dual-functional catalysts, Castillo Marcano et al. [53] investigated the CeO_2/BaO/Pt catalytic system. The active oxides, CeO_2 and BaO, the former with oxidative properties and the latter with NO_x storage capability, were individually prepared and then mixed to form a "physical mixture," or they were simultaneously synthesized to obtain a solid solution through the so-called "co-synthesis" method. Pt was added in a subsequent step. The activity toward soot oxidation revealed that a physical mixture of CeO_2 and BaO allows to obtain more performing catalysts than the co-synthesis route, the former reaching a peak temperature of soot oxidation 25 °C lower than the latter. The Pt addition to the two catalysts further reduces their peak temperatures by around 30 °C in both cases.

Another class of Ce-containing materials proposed as soot oxidation catalysts is that of MnO_x-CeO_2 mixed oxides [54]. The good catalytic activity of Mn-Ce solid solutions is generally attributed to the formation of oxygen vacancies related to the generation of Ce^{3+}. Recently, Jampaiah et al. [55] prepared Mn_3O_4/CeO_2 catalysts in the form of dispersed Mn_3O_4 nanoparticles supported on CeO_2 microspheres. They

varied the Mn_3O_4 load. The maximum soot oxidation activity, found with 20% Mn_3O_4 load, was attributed to the easiest generation of active oxygen species and to the best synergistic interaction at the interface between CeO_2 and Mn_3O_4, in turn due to the optimal deformation of the CeO_2 structure and the subsequent formation of oxygen vacancies. A high stability was also reported for these composite catalysts. In agreement, Sartoretti et al. [56] found that 5% Mn-doped CeO_2 shows a good and stable (after repeated cycles) activity for soot oxidation related to the ability of this catalyst to regenerate the most active defect sites.

To sum up, a wide variety of elements with different features (size, valence state, reducibility, mobility, melting point of their salts, etc.) has been proposed to promote the activity of CeO_2 toward soot oxidation. The main positive effects of their addition to ceria are as follows: enhanced formation of surface active species through the creation of oxygen vacancies/defect sites; improvement in the soot-catalyst contact conditions; introduction of an additional functionality cooperating in NO_x-assisted soot oxidation.

6.5 Other Catalysts

Although CeO_2, pure and in combination with other elements, is the most widely used catalyst for soot oxidation, several other compounds have been proposed as briefly reviewed in this section.

Wagloehner and Kureti [57] described a scheme of global reactions for the mechanism of soot oxidation on Fe_2O_3. According to this scheme, oxygen is transferred from the catalyst surface to soot by contact points. The resulting oxygen defects of the catalyst surface are refilled either by surface migration and final reoxidation by gas-phase oxygen or by diffusing bulk oxygen. The oxygen deficiency of the lattice is balanced by migration of oxygen from the surface or subsurface to the bulk of the catalyst. The authors also found that the local temperature in the catalyst-soot mixture strongly depends on the amount of catalyst (i.e., the catalyst acts as a temperature buffer). Thus, there exists an optimum catalyst/soot ratio reflecting a compromise between a high number of contact points (high catalyst mass) and a low heat capacity (low catalyst mass).

Perovskite-based catalysts were investigated for soot oxidation (see, e.g., [58–60]). Bensaid et al. [60] prepared several perovskites by the "solution combustion synthesis" (SCS) method described in Civera et al. [61]. They identified $Ce_{0.5}Pr_{0.3}La_{0.2}CrO_3$ as the most promising catalyst and demonstrated the feasibility of its deposition on a DPF.

As reported in Sect. 6.4, the addition of silver to ceria has positive effects on soot oxidation. Silver was also added to ZrO_2 by Haneda and Towata [62]. These authors attributed the outstanding performance of Ag nanoparticles supported on ZrO_2 in loose contact with soot to the good solid-solid contact and to the effective migration of active oxygen species from catalyst to soot. Ag was also supported on yttria-stabilized zirconia (YSZ) [63], and results showed a synergistic effect between the

silver mobility and the availability of active oxygen species from the YSZ bulk, which leads to an improved activity with respect to pristine YSZ [64, 65].

Ag- and Ru-based catalysts were investigated by Castoldi et al. [66] for the simultaneous removal of soot and NO_x, and their behavior was compared with that of a model Pt-Ba/Al_2O_3 catalyst. It was found that both the Ag- and Ru-based formulations are active in soot oxidation, more than the traditional Pt-containing catalyst. In addition, the Ru-based sample showed remarkable performances in the deNO_x-desoot activity.

A catalyst for highly efficient NO_x capture and soot combustion was prepared by Dou et al. [67] in the form of a three-dimensional nanosheet array with small-sized active Co_3O_4 phase (5.7 nm) highly dispersed on a Mg/Al-oxide matrix.

The positive effect of alkali metals on catalytic soot oxidation, already discussed for CeO_2 in Sect. 6.4, has largely been demonstrated also for other materials. The promotion effect of potassium on the activity of transition metal (Mn, Fe, Co) spinels was reported by Legutko et al. [68]. These authors found that the location of the potassium promoter in the bulk, more than on the surface of the spinels, markedly lowers the onset temperature of soot oxidation.

Mul et al. [69] reported that the high soot oxidation activity in loose contact of catalytic systems containing an alkali metal chloride (KCl or CsCl or LiCl) and $CuMoO_4$ (or $CuWO_4$ or copper vanadates) can be ascribed to the formation of volatile copper chlorides. More specifically, it can be partially explained by the mobility and volatility of these compounds, resulting in an intimate contact between soot and catalyst. However, despite copper chlorides can be formed by reaction between KCl (which serves as a chlorine supplier) and $CuMoO_4$, the application of supported Cu/K/Mo/Cl catalysts was considered questionable due to the possible loss of activity caused by evaporation and decomposition of the active species.

Carrascull et al. [70] investigated KNO_3/ZrO_2 catalysts with different compositions, i.e., KNO_3 concentrations (in g of KNO_3/g of catalyst). They reported that the difference in temperature of the maximum soot combustion rate between loose contact and tight contact decreases with increasing KNO_3 concentration (in particular, from 95 °C with a concentration equal to 0.25% to 10 °C with 20%). This trend was attributed to the improved contact promoted by molten potassium nitrate.

Sui et al. [71] reported that KNO_3 greatly lowers the soot onset ignition temperature for Co-Sr catalysts. In agreement with Carascull et al. [70], they found that the soot-catalyst contact is strongly improved above the melting point of KNO_3.

An and McGinn [72] studied the wet contact and reported that the high activity they found for potassium-containing oxides is due to the intimate contact between soot and potassium cations caused by polar solvents.

Courcot and coworkers [73, 74] investigated the effect of potassium on both TiO_2 and ZrO_2 supports also in combination with copper. They reported that potassium not only favors the solid-solid contact, but also promotes the release of active oxygen species [74] and enhances the redox properties of copper [73, 74]. Thus, the role of the alkaline metal is not limited to improving the soot-catalyst contact conditions.

Galdeano et al. [75] explored cesium and other alkaline (Li and K) nitrates supported on hydrous zirconium. Under operative conditions similar to the catalyst

behavior in the engine (loose contact) and in the presence of NO, the activity correlates with the electropositive character of the metal. The catalyst with cesium nitrate becomes active at a temperature lower than its melting point. It exhibits a combustion temperature of 364 °C within the values required for the catalyst to operate in the real case of an automobile. The catalyst with lithium nitrate becomes active at a temperature higher than its melting point, and the same occurs for the catalyst with potassium nitrate.

6.6 NO_x Assistance to Bridge the Tight-Loose Contact Gap

Diesel exhaust gases also contain nitrogen oxides which, in order to comply with the emission regulations, must be abated. However, as already mentioned in the previous two sections (mostly in Sect. 6.4), they positively affect soot oxidation.

Kaspera et al. [76] highlighted the role of NO_2 acting as an oxygen carrier from catalyst to soot lowering the temperature of 50% conversion in loose contact by ~100 °C, thus bridging the tight-loose contact temperature gap in NO_x-assisted catalytic oxidation of soot. This was observed on vanadium-doped cryptomelane $K_xMn_8O_{16}$ nanorods. It was found that the incorporation of vanadium into the cryptomelane framework substantially increases the desoot activity by promoting beneficial NO oxidation to NO_2. Two types of oxygen transport were distinguished: through space and across the surface. In the first case, NO_2 acts as an oxygen carrier from catalyst toward soot (through space transport). This situation corresponds to the experiments carried out in loose contact, especially in contactless modes. On the other hand, in tight contact, the oxygen reactive species are transported across the surface from the sites of oxygen activation and formation of oxygen reactive species toward the soot-catalyst contact points, where catalytic combustion actually takes place. This process is conventionally regarded as oxygen surface migration or spillover, as no auxiliary molecule is involved in the oxygen surface transport.

Likewise, Legutko et al. [68] found, for K-promoted transition metal spinels, that the difference in activity between tight contact and loose contact can be bridged in the presence of NO due to its transformation into NO_2, which acts as an oxygen carrier from the catalyst surface to the soot particles. The same was reported by Jakubek et al. [77] for nanostructured potassium-manganese oxides decorated with 1% Pd.

The effects of NO and NO_2 addition were investigated by Zhang et al. [78] for Pt/MnO_x-CeO_2 catalysts in tight and loose contact with soot. It was found that the promotion effects of NO_x are not exhibited in tight contact due to the inhibition of nitrate formation by the soot coverage on the catalyst surface. On the other hand, in loose contact, NO, more than NO_2, promotes the formation of surface nitrates which decompose providing surface active species able to accelerate soot oxidation.

Shen et al. [79] reported that, in tight contact, the "NO_2 assistance" to soot combustion on Fe-Ce-O catalysts is limited due to the inhibition of NO oxidation. Nevertheless, when soot is gradually consumed, the solid-solid contact becomes loose, thus resulting in an improvement of NO oxidation to NO_2.

Christensen et al. [80] found similar results for various metal and metal oxide catalysts. They observed a marked enhancement of the rate constant of soot oxidation in loose contact in the presence of NO_2. Among the tested catalysts, Cr_2O_3 is the most active one.

Zouaoui et al. [81] determined the kinetic parameters of soot oxidation in both loose and tight contact with CeO_2 under O_2 and NO/O_2. The activation energy was found to be strongly dependent on the type of contact in the presence of oxygen and to slightly depend when NO is also used.

6.7 Nanostructured Ceria Morphologies

In a real DPF, the catalytic activity is not the only important feature: an engineered morphology has to be designed to achieve better results [82]. It has been demonstrated that the catalytic activity of ceria toward soot oxidation depends on the contact points obtained at the interface between soot and catalyst and on the availability of active surface oxygen [83]. Both issues can be managed by modifying the morphology [82], thus also exposing more active crystalline planes [50, 84].

A CeO_2 morphology with fibrous structure has been proposed to maximize the contact between catalyst and soot particles [85, 86]. Despite their low specific surface area (SSA), these fibers have a filamentous structure that enhances the number of soot-fiber contact points and, in some cases, show better performances than foamy or higher SSA nanopowders. In other words, tailored morphologies can be achieved even with low specific areas. This proves that the specific surface area is not the only important factor in solid-solid catalysis. The fact that the sizes of soot particles and catalyst grains often have different orders of magnitude leads to a poor accessibility of the soot particles to the inner pores of the catalyst, and this aspect could be rate-limiting especially at low temperatures [85].

Miceli et al. [82] compared three CeO_2 morphologies, shown in the field-emission scanning electron microscopy (FESEM) images of Figs. 6.9, 6.10, and 6.11, in both

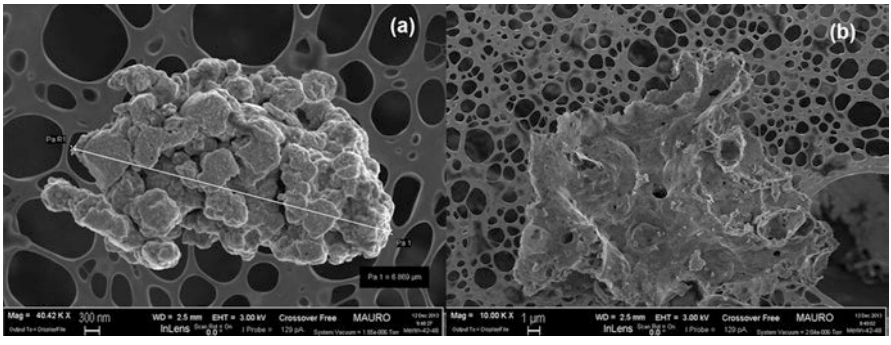

Fig. 6.9 FESEM images of ceria SCS nanopowders: (**a**) high and (**b**) low level of magnification [82]

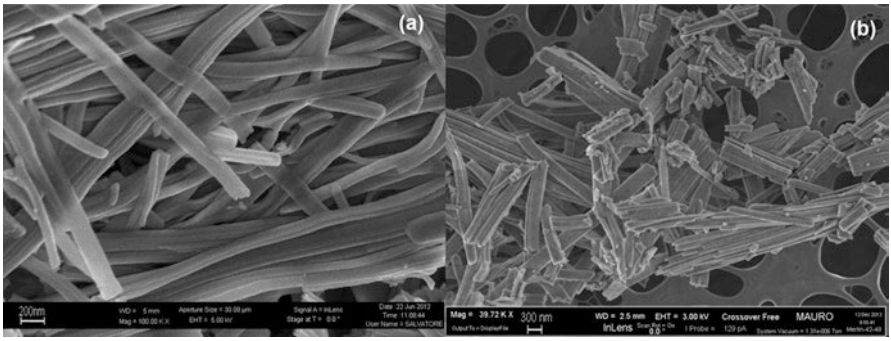

Fig. 6.10 FESEM images of ceria nanofibers: (**a**) high and (**b**) low level of magnification [82]

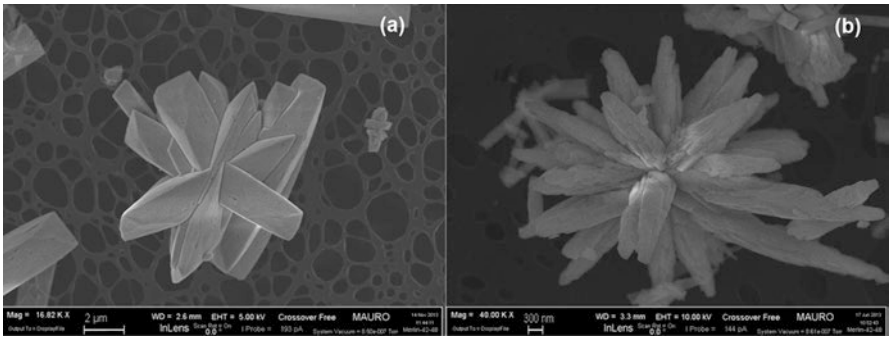

Fig. 6.11 FESEM images of ceria SA stars at different residence times inside the reactor in hydrothermal conditions: (**a**) 12 h and (**b**) 24 h [82]

tight and loose contact with soot: foamy structured CeO_2 prepared by the solution combustion synthesis (SCS) method (Fig. 6.9), nanofibers (Fig. 6.10), and self-assembled (SA) stars (Fig. 6.11).

They found that three-dimensional self-assembled stars, which have both a high specific surface area (105 m^2/g) and a high availability of contact points, give the best results especially in loose contact. Indeed, in tight contact, the mechanical force generates a particularly close contact between soot and catalyst, and thus, the advantages of the morphology are less important. Conversely, in loose contact, the morphology plays a more relevant role: nanofibers, despite the almost null surface area, exhibit an activity almost equivalent to that of SCS nanopowders. On the other hand, the high porosity of self-assembled stars provides more adsorbed oxygen to the contact points between soot and catalyst, which is likely to be in a sufficient amount to fully exploit this oxygen availability. Figure 6.12 shows the FESEM images representing a loose mixture of ceria SA stars and soot at different levels of magnification.

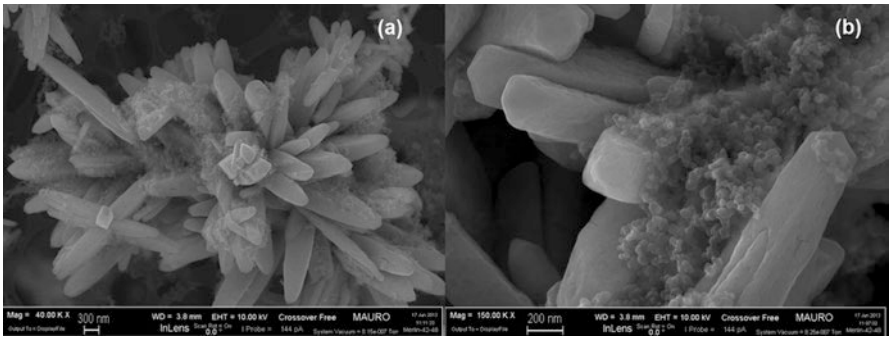

Fig. 6.12 FESEM images representing a loose mixture of ceria SA stars and soot: (**a**) low and (**b**) high level of magnification [82]

Miceli et al. [87] also found that self-assembled stars have a greater availability of oxygen vacancies and undergo more efficient redox cycles with a higher oxidative capability.

Zhang et al. [88] highlighted the role of the morphology of CeO_2 in loose contact, when the different physicochemical properties greatly influence the activity toward soot combustion also in the presence of NO. They found that nanorods perform better than nanoparticles and flakes due to a higher surface area and a higher adsorption of oxygen species on the surface.

On the contrary, Piumetti et al. [89] observed a "surface insensitivity" of CeO_2 with different textural and morphological properties, also dispersed on ZSM5, in both loose and tight contact at low temperatures, and they attributed this feature to the presence of adsorbed species (like hydroxyl groups, inert molecules, etc.) on the solid surface weakening the reactant-catalyst surface interaction through masking of the active sites. Nevertheless, above 410 or 370 °C (in loose or tight contact, respectively), a "surface sensitivity" was observed.

The same authors also investigated various CeO_2 morphologies and three contact conditions: tight contact, loose contact (with a 1–2 min mixing time), and a so-called "prolonged" loose contact (with a 30 min mixing time) [86]. In tight contact, nanofibers, having a low specific surface area, exhibit an onset temperature almost comparable to the one achieved with SCS nanopowders. An optimal contact between soot and catalyst is reached when the network of nanofibers has average pore diameters of the same order of magnitude as the soot particle ones. Conversely, sticks and flakes have excessive size, and a macroporous framework is formed, which poorly adapts to the soot particle average size. An important feature of SCS nanopowders is their better selectivity toward CO_2 than all the other morphologies due to the high specific surface area which provides a greater reactivity toward gaseous species, namely CO. The prolonged loose contact was adopted because fibers, sticks, and flakes are harder than SCS nanopowders, which are very soft. The latter are very easily and rapidly mixed up with the soot particles, while fibers require a longer time to be fully covered by the soot particles. In these conditions, even the

selectivity to CO_2 of nanofibers is satisfactory and not much different from that of SCS nanopowders. In loose conditions (i.e., conditions which bring out the easier mixing of SCS nanoparticles with soot, due to their softness), no clear preeminence of either powders or fibers was observed. Even sticks and flakes approach the activity of SCS nanopowders. This encourages to better investigate the interaction between the morphology and the real contact conditions between soot and catalyst in DPFs and to tailor the catalytic support to enhance this contact while still minimizing the contribution of the catalytic layer to the pressure drop across the filter.

The effect of the ceria morphology was also reported by Aneggi et al. [90]. Nanocubes, which expose {100} surface, and nanorods, which expose {100}, {110}, and in part {111} surfaces, show a higher catalytic activity than conventional polycrystalline ceria, which exposes mainly {111} surface. Very interestingly, aged catalysts show irregular truncation of edges and corners and development of more reactive surface combinations in all crystal shapes at the expense of the specific surface area.

Cheng et al. [91] investigated a series of three-dimensionally ordered macroporous (3DOM) $Ce_{0.9-x}Fe_{0.1}Zr_xO_2$ catalysts with different Ce/Zr ratios. These catalysts were prepared by a colloidal crystal template method. The 3DOM unique structure promotes the contact of particulate matter (PM) with the active sites of the catalyst. The high Ce^{3+}/Ce^{4+} ratio, the amount of chemisorbed oxygen species, the good low-temperature reducibility, and the abundance of acidic sites were considered responsible for the excellent catalytic efficiency of the $Ce_{0.85}Fe_{0.1}Zr_{0.05}O_2$ sample for the simultaneous removal of PM and NO_x.

In conclusion, catalytic soot oxidation is a surface-dependent reaction. The use of catalysts with morphologies that maximize the extent of the soot-catalyst interface, even if this could be coupled to a low specific surface area, is recommended to achieve a good oxidation activity. An opportune choice of preferentially exposed crystal planes, more active than others, can further improve the catalytic performance.

6.8 Filters Coated with Nanostructured Catalysts

The importance of the soot-catalyst contact to an effective catalytic combustion of soot has also been highlighted by experiments carried out on both filters and "flow-through" monoliths coated with nanostructured catalysts. To examine what happens on the filter under as realistic as possible regeneration conditions is indeed crucial. As shown by Hinot et al. [92] with platinum nanoparticles, in going from catalyst-doped soot to a thin deposit (5–10 μm) of soot on a catalytic layer, the catalytic effectiveness may drastically drop. In particular, they found that the reduction in soot oxidation temperature with respect to thermal oxidation decreases from 140–250 °C (catalyst-doped soot) to 10–40 °C (soot deposited on a catalytic layer), and this was attributed to the increased "average" distance between soot and catalyst particles.

Fino's group prepared catalytic filters on the basis of a series of nanostructured perovskite catalysts [60, 93–95]. The preparation method employed in these works is the in situ solution combustion synthesis (SCS). A nanostructured and foamy catalyst coating over the DPF was obtained, and this issue was considered as an essential prerequisite not only for a good soot-catalyst contact, but also for a rather low-pressure drop throughout the channel walls.

More recently, perovskite-based flow-through monoliths were successfully tested for soot oxidation by Tang et al. [96]. In this work, monolithic catalysts were prepared by a two-step procedure. Cordierite monoliths were first washcoated with porous hollow γ-Al_2O_3 nanoparticles by dip coating. Active components, i.e., nanometric $LaKCoO_3$ or $LaCoO_3$ perovskite-type complex oxides, were then loaded by impregnation of the as-prepared monoliths with corresponding aqueous solution of metal salts. For comparison, the one-step method without the alumina coating was also investigated. It was found that the introduction of the γ-Al_2O_3 washcoat is crucial to greatly increase the surface area of the monolithic cordierite. This allows to increase the loading amount of active components and also to enhance their dispersion on the surface of the monolith, thus leading to improved conditions of soot-catalyst contact. The CO_2 concentration curves of Fig. 6.13, recorded during soot combustion over different monolithic catalysts, show that the presence of the γ-Al_2O_3 washcoat allows better performance.

The fact that the production of large-scale catalytic surfaces inside the DPF plays a key role in determining the efficiency of the soot-catalyst contact was also proven by Zhou et al. [97], who proposed a low-cost electroless coating approach that allows in situ growth of nanostructured metal crystals inside the pores of ceramic filters. Results from nanoscale imaging characterization and element-specific energy dispersive X-ray (EDX) spectra demonstrated the presence of a well-dispersed

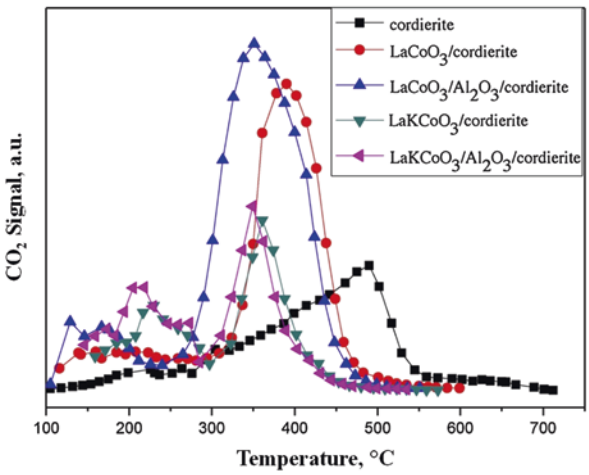

Fig. 6.13 CO_2 concentration curves recorded during soot combustion over different monolithic catalysts [96]

catalyst (Pt) throughout the filter, on the channel surfaces and inside the pores, resulting in a substrate that is highly active toward soot oxidation. According to the proposed method, the shape of the nanostructured catalyst can be tuned, from spheroid particle, rod-like wire to fern-like dendritic structure, by varying the starting reactant concentration and the length of the deposition time. The scanning electron microscopy (SEM) images of Fig. 6.14 show (a) the bare DPF sample and (b–d) Pt-decorated DPF samples, with Pt nanoparticles obtained starting from two different values of reactant concentration, (b) lower and (c) higher, and (d) Pt dendrites (at the higher value of reactant concentration).

The role of the catalyst shape in affecting the efficiency of the contact with soot was investigated, also at the filter level, by Kumar et al. [85], with a focus on nanostructured ceria catalysts. They found that nanofibers are very active with respect to other ceria morphologies, due to their arrangement in a network that enhances the number of soot-fiber contact points. The main advantage given by the nanofiber-catalyzed DPF, with respect to the other investigated morphologies, is related to the onset temperature. This temperature is 150 °C lower than the onset temperature of the un-coated DPF and more than 50 °C lower than the onset temperature of the DPF catalyzed with ceria through in situ SCS.

Filters and flow-through monoliths coated with nanostructured ceria or ceria-based materials were also investigated in more recent works [3, 4, 7, 8, 20, 98].

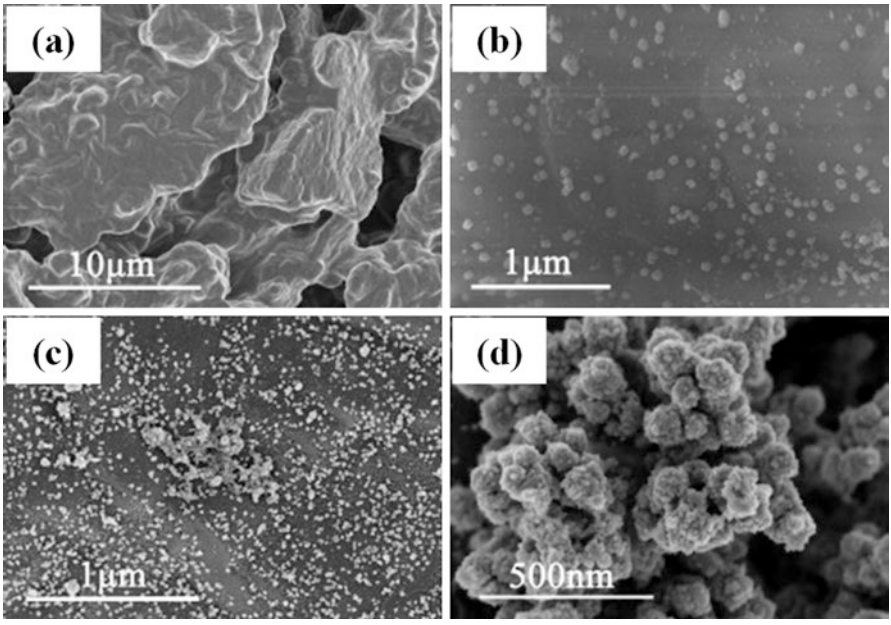

Fig. 6.14 SEM images of the Pt-decorated DPF samples: (**a**) bare filter; Pt nanoparticles obtained starting from two different values of reactant concentration, (**b**) lower and (**c**) higher; (**d**) Pt dendrites (at the higher value of reactant concentration) [97]

Nascimento et al. [7] used the sol-gel methodology to synthesize Ce-Fe binary mixed oxide catalysts (CeO_x/FeO_y). Cordierite monoliths were coated with the CeO_x/FeO_y catalysts. Samples of the cordierite coated with the binary mixed oxides were doped with Ag nanoparticles (addition of 5 wt.%). CeO_x/FeO_y- and $Ag/CeO_x/FeO_y$-coated ceramics were tested for their ability to reduce the soot emission during diesel combustion in a stationary engine. It was found that the silver-doped coating allows better performance as a result of both a relatively good soot-catalyst contact and an effective migration of active oxygen species from the catalyst to soot.

Quiles-Díaz et al. [20] deposited a nanosized 2% CuO/ceria-zirconia catalyst on ceramic DPFs using a simple and organic solvent-free procedure. The filter was simply dipped into an aqueous solution of the catalyst. The adopted procedure allowed to obtain a non-continuous deposit of catalyst on the channel walls, thus preventing the blocking of the filter pores. The regeneration performance of the catalyst-coated DPF is well simulated by the loose contact mode (see Fig. 6.4 in Sect. 6.2). This suggests that a rather weak soot-catalyst contact is established inside the filter under the conditions investigated.

To mimic the soot-catalyst contact achieved inside a real filter, Rico Pérez and Bueno-López [3] loaded nanoparticles of an optimized ceria-praseodymia active phase on silicon carbide (SiC) DPFs and designed an experimental set-up where a suspension of soot particles in air is forced to pass through the filter, thus simulating the filtering process in a real exhaust pipe. Results of regeneration tests performed at different soot loads (while keeping constant the catalyst load) allowed to identify a critical catalyst/soot ratio below which catalytic regeneration is hindered. This was attributed to the weakening of the soot-catalyst contact with increasing soot load. It was argued that the first soot particles loaded have more chances to come into contact with catalyst particles than particles loaded afterward. However, the link between the critical catalyst/soot ratio and the localization of contacted and non-contacted soot entities inside the filter was not elucidated.

A deep investigation of the effect of the catalyst/soot ratio on the "regime" of regeneration of SiC DPFs washcoated with nanometric ceria particles was performed in Di Sarli et al. [4]. The dip-coating procedure adopted for the deposition of ceria, along with the limited catalyst load and the nanometric size of the CeO_2 particles, ensured a high dispersion with a deep penetration of the catalyst into the (macro)pores of the filter walls. Indeed, in order to preserve the filtration properties of the bare support and, at the same time, promote the soot-catalyst contact inside the filter walls, the accumulation of a washcoat layer on top of the channel walls was prevented, thus ensuring the accessibility of soot to the pores of the filter. Results showed that, as the catalyst/soot ratio is decreased (i.e., the soot load is increased), a transition occurs from a regime of "almost purely catalytic regeneration" to a regime of "catalyst-assisted thermal regeneration." In the former regime, most of the soot is trapped inside the pores of the filter walls, thus coming into intimate contact with highly dispersed catalyst. As a consequence, regeneration occurs via the catalytic path at low temperatures. In the latter regime, most of the soot is accumulated in the form of a rather thick cake layer (15–20 μm) on top of the channel walls. The soot cake is substantially segregated from the catalyst and, as such, it

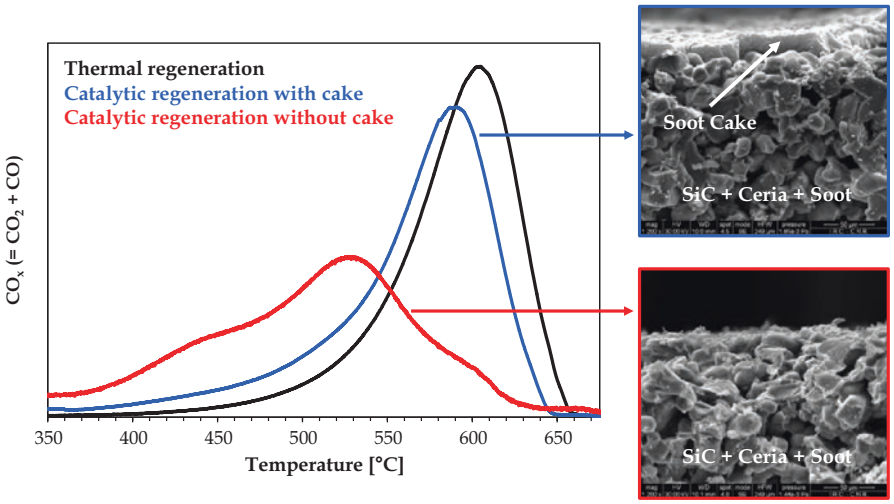

Fig. 6.15 Concentration of CO_x (=CO_2 + CO) versus filter temperature as recorded during three heating-ramp regeneration tests: thermal regeneration test, catalytic regeneration test with cake, and catalytic regeneration test without cake—the SEM images on the right-hand side show the cross section of a channel of the ceria-coated DPF with cake (top image) and without cake (bottom image) [4]

burns via the thermal path at high temperatures. Figure 6.15 is the graphical abstract of this work. It shows the plots of the concentration of CO_x (=CO_2 + CO) versus the filter temperature as recorded during three heating-ramp regeneration tests: thermal regeneration, catalytic regeneration with cake (high soot load and, thus, low catalyst/soot ratio), and catalytic regeneration without cake (low soot load and, thus, high catalyst/soot ratio). The images on the right-hand side are SEM images showing the cross section of a channel of the ceria-coated DPF with cake (top image) and without cake (bottom image).

This figure shows that, once assured a good catalyst dispersion inside the pores of the filter walls, in order to optimize the soot-catalyst contact, thus making regeneration of the DPF a truly catalytic process, it is essential to minimize/avoid the formation of the cake layer. This conclusion is supported further by the results of CFD-based simulations of soot combustion dynamics in a catalytic DPF showing that, once assumed all the soot trapped inside the filter walls to be in contact with the catalyst, fast and at the same time "safe" (i.e., low temperature) regeneration is not possible [99–101] unless the accumulation of soot as cake on top of the catalytic walls is prevented [101, 102].

As highlighted in Sect. 6.1, after the filtration stage, soot is trapped mostly in the form of cake. The results of Fig. 6.15, thus, pave the way to the passage to a continuous regeneration mode for catalytic DPFs, with combustion of soot occurring during (and not after) filtration, thus avoiding excessive soot storage inside the filter as cake.

In order to investigate the potential of (nano)ceria-coated DPFs for continuous regeneration, Di Sarli et al. [98] carried out isothermal regeneration tests—at temperature ranging from 200 to 600 °C—on filters loaded with a very low amount of soot suitably chosen to minimize the formation of the cake layer. Results showed that 475 °C is the minimum temperature at which the soot trapped inside the filter is burned off (and, thus, the filter is regenerated) via the catalytic path. At this temperature, the catalytic filter maintains substantially the same performance over repeated cycles of soot loading and regeneration, indicating that the thermal stability of the ceria catalyst is preserved. This issue was also confirmed by the outcomes of filter characterization.

The intrinsic activity of ceria can be enhanced through doping with a proper active metal, thus further decreasing the filter regeneration temperature to values included in the operative range of diesel exhausts (200–350 °C).

The potential for continuous regeneration was also envisaged in Wagloehner et al. [103] from temperature-programmed oxidation (TPO) studies on a filter coated with a nanosized Mn_3O_4 catalyst originated from flame spray pyrolysis (FSP-Mn_3O_4). Figure 6.16 was obtained from the graphical abstract of this work: the major part of the soot trapped inside the filter (around 80%) is in weak contact with the catalyst causing oxidation above 400 °C only, whereas the minor fraction of soot is in intimate contact with the catalyst evoking conversion already between 180 and 350 °C.

It is worth saying that structured configurations alternative to ceramic wall-flow filters have also been proposed. For instance, Bruneel et al. [104] prepared and tested a three-layer metallic soot filter coated with a CeO_2 buffer layer (used as

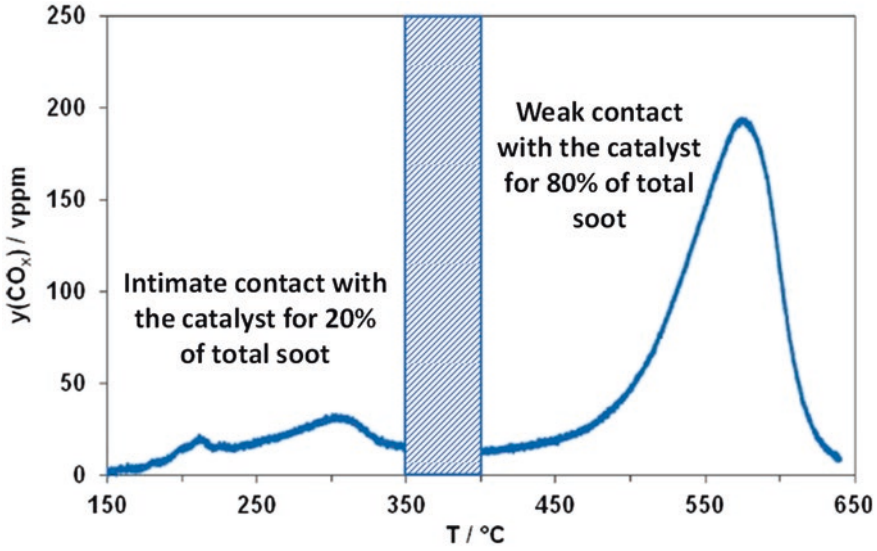

Fig. 6.16 TPO results obtained on a filter coated with a nanosized Mn_3O_4 catalyst originated from flame spray pyrolysis (FSP-Mn_3O_4) [103]

antioxidant) and a soot oxidation catalyst based on copper, molybdenum, and cerium oxides. More recently, Miró and coworkers developed novel structures based on ceramic papers [105, 106]. These are sheets of ceramic fibers (SiO_2-Al_2O_3) used as a support for the active phase. The best results were obtained with a mixed oxide containing Co, Ba, and K, showing a good dispersion onto the ceramic fibers [105].

6.9 Conclusions and Outlook

In this chapter, the main critical issue for regeneration of catalytic DPFs has been addressed, i.e., the efficiency of the contact in the solid-solid reaction between soot and catalyst, highlighting the close correlation of this issue with size and morphology of the catalyst particles.

The different types of soot-catalyst contact simulated at lab-scale have been analyzed in detail, ranging from the tight (or supertight) contact, which maximizes the contact points and provides information on the reaction mechanism, to the loose contact, which better reproduces the conditions of a real process of regeneration of catalytic DPF.

It has been highlighted that, even with a catalyst exhibiting an outstanding intrinsic activity, a poor contact with soot can strongly limit the performance. Indeed, when the soot-catalyst contact is weak, attempts to improve the oxygen mobility inside the catalyst lattice, thus increasing the soot oxidation rate, through suitable formulations and/or doping, may be in vain if the active oxygen is unable to reach the soot particle. On the other hand, an improved contact between the two solids allows enhancing all the phenomena occurring at the soot-catalyst interface. In this context, the nanosize of the catalyst particles plays a crucial role and, as such, represents a key factor for the production of highly performing soot oxidation catalysts.

Although the presence of nitrogen oxides in diesel exhaust gases can help to bridge the gap between loose and tight contact, it is essential to maximize the soot-catalyst contact inside the DPF, thus approaching tight conditions. In this regard, the increase of the number of contact points through the formation of special catalyst morphologies has been shown. A high exposure of active crystal planes of the catalyst particles provides better results than a high specific surface area related to a great catalyst porosity, since the soot particles cannot penetrate into the catalyst pores. The best results have been obtained when the size of the spaces created in the special catalyst morphology (for instance, a network of nanofibers) is of the same order of magnitude as the soot particle size.

As far as the catalyst deposition on the DPF is concerned, the importance of obtaining a high dispersion with a deep penetration of the catalyst nanoparticles into the pores of the filter walls has been highlighted. In addition, the critical issue of the amount of soot trapped inside the catalytic filter (i.e., the soot/catalyst ratio) has been addressed. The formation of a soot cake layer on top of the channel walls is not recommended, as it determines a poor contact with the catalyst located inside the pores of the walls. An almost totally catalytic regeneration of the DPF can more

easily take place at lower temperatures if soot is mostly located inside the filter pores. If a reasonably low temperature of the catalytic process can be achieved, a continuous regeneration can be supposed: the newly filtered soot particles replace the quickly burning soot particles in the DPF pores, with an evident advantage also for the engine never working with a clogged filter.

The development of novel catalytic DPFs operating under continuous regeneration conditions is, thus, the most interesting challenge to be addressed in coming years. It involves the development of novel catalyst configurations showing improved contact conditions during filtration, a high activity at relatively low temperatures, and a high long-term stability.

References

1. P. Tandon, A. Heibel, J. Whitmore, N. Kekre, K. Chithapragada, Measurement and prediction of filtration efficiency evolution of soot loaded diesel particulate filters. Chem. Eng. Sci. **65**, 4751–4760 (2010)
2. K. Yang, J.T. Fox, R. Hunsicker, Characterizing diesel particulate filter failure during commercial fleet use due to pinholes, melting, cracking, and fouling. Emiss. Control Sci. Technol. **2**, 145–155 (2016)
3. V.R. Pérez, A. Bueno-López, Catalytic regeneration of diesel particulate filters: comparison of Pt and CePr active phases. Chem. Eng. J. **279**, 79–85 (2015)
4. V. Di Sarli, G. Landi, L. Lisi, A. Saliva, A. Di Benedetto, Catalytic diesel particulate filters with highly dispersed ceria: effect of the soot-catalyst contact on the regeneration performance. Appl. Catal. B Environ. **197**, 116–124 (2016)
5. L. Rocher, T. Seguelong, V. Harle, M. Lallemand, M. Pudlarz, M. Macduff, New generation fuel borne catalyst for reliable DPF operation in globally diverse fuels. SAE Technical Paper 2011-01-0297 (2011)
6. L. De Marzi, A. Monaco, J. De Lapuente, D. Ramos, M. Borras, M. Di Gioacchino, S. Santucci, A. Poma, Cytotoxicity and genotoxicity of ceria nanoparticles on different cell lines in vitro. Int. J. Mol. Sci. **14**, 3065–3077 (2013)
7. L.F. Nascimento, J.F. Lima, P.C. de Sousa Filho, O.A. Serra, Control of diesel particulate emission based on $Ag/CeO_x/FeO_y$ catalysts supported on cordierite. Chem. Eng. J. **290**, 454–464 (2016)
8. V. Di Sarli, G. Landi, L. Lisi, A. Di Benedetto, Highly dispersed ceria for catalytic regeneration of diesel particulate filter. Adv. Sci. Lett. **23**, 5909–5911 (2017)
9. C. Su, Y. Wang, A. Kumar, P.J. McGinn, Simulating real world soot-catalyst contact conditions for lab-scale catalytic soot oxidation studies. Catalysts **8**, 247 (2018)
10. S. Cao, F.F. Tao, Y. Tang, Y. Li, J. Yu, Size- and shape-dependent catalytic performances of oxidation and reduction reactions on nanocatalysts. Chem. Soc. Rev. **45**, 4747–4765 (2016)
11. M. Valden, X. Lai, D.W. Goodman, Onset of catalytic activity of gold clusters on titania with the appearance of nonmetallic properties. Science **281**, 1647–1650 (1998)
12. F.Y. Kwong, A. Klapars, S.L. Buchwald, Copper-catalyzed coupling of alkylamines and aryl iodides: an efficient system even in an air atmosphere. Org. Lett. **4**, 581–584 (2002)
13. F.Y. Kwong, S.L. Buchwald, Mild and efficient copper-catalyzed amination of aryl bromides with primary alkylamines. Org. Lett. **5**, 793–796 (2003)
14. H. Rao, Y. Jin, H. Fu, Y. Jiang, Y. Zhao, A versatile and efficient ligand for copper-catalyzed formation of C-N, C-O, and P-C bonds: pyrrolidine-2-phosphonic acid phenyl monoester. Chem. Eur. J. **12**, 3636–3646 (2006)

15. B.R. Stanmore, J.F. Brilhac, P. Gilot, The oxidation of soot: a review of experiments, mechanisms and models. Carbon **39**, 2247–2268 (2001)
16. A. Bueno-López, Diesel soot combustion ceria catalysts. Appl. Catal. B Environ. **146**, 1–11 (2014)
17. L. Hensgen, K. Stöwe, Soot-catalyst contact studies in combustion processes using nanoscaled ceria as test material. Catal. Today **159**, 100–107 (2011)
18. P. Ciambelli, M. D'Amore, V. Palma, S. Vaccaro, Catalytic oxidation of an amorphous carbon black. Combust. Flame **99**, 413–421 (1994)
19. J.P.A. Neeft, M. Makkee, J.A. Moulijn, Catalytic oxidation of carbon black—I. Activity of catalysts and classification of oxidation profiles. Fuel **77**, 111–119 (1998)
20. S. Quiles-Díaz, J. Giménez-Mañogil, A. García-García, Catalytic performance of CuO/$Ce_{0.8}Zr_{0.2}O_2$ loaded onto SiC-DPF in NO_x-assisted combustion of diesel soot. RSC Adv. **5**, 17018–17029 (2015)
21. J.M. Christensen, J.D. Grunwaldt, A.D. Jensen, Importance of the oxygen bond strength for catalytic activity in soot oxidation. Appl. Catal. B Environ. **188**, 235–244 (2016)
22. J. Liu, Z. Zhao, C.M. Xu, H. Wang, Study of the catalytic combustion of diesel soot over nanometric lanthanum-cobalt mixed oxide catalysts. React. Kinet. Catal. Lett. **87**, 107–114 (2005)
23. E. Aneggi, V. Rico-Perez, C. de Leitenburg, S. Maschio, L. Soler, J. Llorca, A. Trovarelli, Ceria-zirconia particles wrapped in a 2D carbon envelope: improved low-temperature oxygen transfer and oxidation activity. Angew. Chemie Int. Ed. **54**, 14040–14043 (2015)
24. E. Aneggi, J. Llorca, A. Trovarelli, M. Aouinea, P. Vernoux, In situ environmental HRTEM discloses low temperature carbon soot oxidation by ceria-zirconia at the nanoscale. Chem. Commun. **55**, 3876–3878 (2019)
25. S.B. Simonsen, S. Dahl, E. Johnson, S. Helveg, Ceria-catalyzed soot oxidation studied by environmental transmission electron microscopy. J. Catal. **255**, 1–5 (2008)
26. L. Soler, A. Casanovas, C. Escudero, V. Pérez-Dieste, E. Aneggi, A. Trovarelli, J. Llorca, Ambient pressure photoemission spectroscopy reveals the mechanism of carbon soot oxidation in ceria-based catalysts. ChemCatChem **8**, 2748–2751 (2016)
27. B. Bassou, N. Guilhaume, K. Lombaert, C. Mirodatos, D. Bianchi, Experimental microkinetic approach of the catalytic oxidation of diesel soot by ceria using temperature-programmed experiments. Part 1: impact and evolution of the ceria/soot contacts during soot oxidation. Energy Fuel **24**, 4766–4780 (2010)
28. B. Bassou, N. Guilhaume, K. Lombaert, C. Mirodatos, D. Bianchi, Experimental microkinetic approach of the catalytic oxidation of diesel soot by ceria using temperature-programmed experiments. Part 2: kinetic modeling of the impact of the ceria/soot contacts on the rate of oxidation. Energy Fuel **24**, 4781–4792 (2010)
29. M. Issa, C. Petit, A. Brillard, J.F. Brilhac, Oxidation of carbon by CeO_2: effect of the contact between carbon and catalyst particles. Fuel **87**, 740–750 (2008)
30. E. Saab, E. Abi-Aad, M.N. Bokova, E.A. Zhilinskaya, A. Aboukaïs, EPR characterisation of carbon black in loose and tight contact with Al_2O_3 and CeO_2 catalysts. Carbon **45**, 561–567 (2007)
31. M. Issa, C. Petit, H. Mahzoul, A. Aboukaïs, J.F. Brilhac, EPR and SEM characterizations of the contact between carbon black and cerium oxide. Top. Catal. **52**, 2063–2069 (2009)
32. P. Sudarsanam, B. Hillary, B. Mallesham, B.G. Rao, M.H. Amin, A. Nafady, A.M. Alsalme, B.M. Reddy, S.K. Bhargava, Designing CuO_x nanoparticle-decorated CeO_2 nanocubes for catalytic soot oxidation: role of the nanointerface in the catalytic performance of heterostructured nanomaterials. Langmuir **32**, 2208–2215 (2016)
33. B. Cui, S. Yan, Y. Xia, K. Li, S. Li, D. Wang, Y. Ye, Y.Q. Liu, $Cu_xCe_{1-x}O_2$ nanoflakes with improved catalytic activity and thermal stability for diesel soot combustion. Appl. Catal. A Gen. **578**, 20–29 (2019)

34. P. Sudarsanam, B. Hillary, M.H. Amin, N. Rockstroh, U. Bentrup, A. Brückner, S.K. Bhargava, Heterostructured copper-ceria and iron-ceria nanorods: role of morphology, redox, and acid properties in catalytic diesel soot combustion. Langmuir **34**, 2663–2673 (2018)
35. A. Bueno-López, K. Krishna, M. Makkee, J.A. Moulijn, Enhanced soot oxidation by lattice oxygen via La^{3+}-doped CeO_2. J. Catal. **230**, 237–248 (2005)
36. C.B. Lim, H. Kusaba, H. Einaga, Y. Teraoka, Catalytic performance of supported precious metal catalysts for the combustion of diesel particulate matter. Catal. Today **175**, 106–111 (2011)
37. J.P.A. Neeft, M. Makkee, J.A. Moulijn, Metal oxides as catalysts for the oxidation of soot. Chem. Eng. J. Biochem. Eng. J. **64**, 295–302 (1996)
38. D. Gardini, J.M. Christensen, C.D. Damsgaard, A.D. Jensen, J.B. Wagner, Visualizing the mobility of silver during catalytic soot oxidation. Appl. Catal. B Environ. **183**, 28–36 (2016)
39. K. Mori, K. Watanabe, T. Sato, H. Yamashita, Environmental transmission electron microscopy study of diesel carbon soot combustion under simulated catalytic-reaction conditions. ChemPhysChem **16**, 1347–1351 (2015)
40. E. Aneggi, J. Llorca, C. de Leitenburg, G. Dolcetti, A. Trovarelli, Soot combustion over silver-supported catalysts. Appl. Catal. B Environ. **91**, 489–498 (2009)
41. S. Liu, X. Wu, W. Liu, W. Chen, R. Ran, M. Li, D. Weng, Soot oxidation over CeO_2 and Ag/CeO_2: factors determining the catalyst activity and stability during reaction. J. Catal. **337**, 188–198 (2016)
42. J.H. Lee, S.H. Lee, J.W. Choung, C.H. Kim, K.Y. Lee, Ag-incorporated macroporous CeO_2 catalysts for soot oxidation: effects of Ag amount on the generation of active oxygen species. Appl. Catal. B Environ. **246**, 356–366 (2019)
43. L. Zeng, L. Cui, C. Wang, W. Guo, C. Gong, Ag-assisted CeO_2 catalyst for soot oxidation. Front. Mater. Sci. **13**, 288–295 (2019)
44. X. Deng, M. Li, J. Zhang, X. Hu, J. Zheng, N. Zhang, B.H. Chen, Constructing nano-structure on silver/ceria-zirconia towards highly active and stable catalyst for soot oxidation. Chem. Eng. J. **313**, 544–555 (2017)
45. G. Corro, A. Flores, F. Pacheco-Aguirre, U. Pal, F. Bañuelos, R. Araceli, A. Zehe, Biodiesel and fossil-fuel diesel soot oxidation activities of Ag/CeO_2 catalyst. Fuel **250**, 17–26 (2019)
46. D. Weng, J. Li, X. Wu, F. Lin, Promotional effect of potassium on soot oxidation activity and SO_2-poisoning resistance of Cu/CeO_2 catalyst. Catal. Commun. **9**, 1898–1901 (2008)
47. A. Alinezhadchamazketi, A.A. Khodadadi, Y. Mortazavi, A. Nemati, Catalytic evaluation of promoted CeO_2-ZrO_2 by transition, alkali, and alkaline-earth metal oxides for diesel soot oxidation. J. Environ. Sci. **25**, 2498–2506 (2013)
48. L. Sui, Y. Wang, H. Kang, H. Dong, L. Dong, L. Yu, Effect of Cs-Ce-Zr catalysts/soot contact conditions on diesel soot oxidation. ACS Omega **2**, 6984–6990 (2017)
49. H. Shimokawa, Y. Kurihara, H. Kusaba, H. Einaga, Y. Teraoka, Comparison of catalytic performance of Ag- and K-based catalysts for diesel soot combustion. Catal. Today **185**, 99–103 (2012)
50. M. Piumetti, S. Bensaid, N. Russo, D. Fino, Investigations into nanostructured ceria-zirconia catalysts for soot combustion. Appl. Catal. B Environ. **180**, 271–282 (2016)
51. V. Rico-Pérez, E. Aneggi, A. Trovarelli, The effect of Sr addition in Cu- and Fe-modified CeO_2 and ZrO_2 soot combustion catalysts. Catalysts **7**, 28 (2017)
52. V. Rico-Pérez, E. Aneggi, A. Bueno-López, A. Trovarelli, Synergic effect of Cu/$Ce_{0.5}Pr_{0.5}O_{2-\delta}$ and $Ce_{0.5}Pr_{0.5}O_{2-\delta}$ in soot combustion. Appl. Catal. B Environ. **197**, 95–104 (2016)
53. S.J. Castillo Marcano, S. Bensaid, F.A. Deorsola, N. Russo, D. Fino, Multifunctional catalyst based on BaO/Pt/CeO_2 for NO_2-assisted soot abatement and NO_x storage. Fuel **149**, 78–84 (2015)
54. Y. Gao, X. Wu, S. Liu, D. Weng, R. Ran, MnO_x-CeO_2 mixed oxides for diesel soot oxidation: a review. Catal. Surv. Jpn. **22**, 230–240 (2018)
55. D. Jampaiah, V.K. Velisoju, D. Devaiah, M. Singh, E.L.H. Mayes, V.E. Coyle, B.M. Reddy, V. Bansal, S.K. Bhargava, Flower-like Mn_3O_4/CeO_2 microspheres as an efficient catalyst for

diesel soot and CO oxidation: synergistic effects for enhanced catalytic performance. Appl. Surf. Sci. **473**, 209–221 (2019)
56. E. Sartoretti, C. Novara, F. Giorgis, M. Piumetti, S. Bensaid, N. Russo, D. Fino, In situ Raman analyses of the soot oxidation reaction over nanostructured ceria-based catalysts. Sci. Rep. **9**, 3875 (2019)
57. S. Wagloehner, S. Kureti, Study on the mechanism of the oxidation of soot on Fe_2O_3 catalyst. Appl. Catal. B Environ. **125**, 158–165 (2012)
58. Y. Teraoka, K. Nakano, S. Kagawa, W.F. Shangguan, Simultaneous removal of nitrogen oxides and diesel soot particulates catalyzed by perovskite-type oxides. Appl. Catal. B Environ. **5**, L181–L185 (1995)
59. A. Mishra, R. Prasad, Preparation and application of perovskite catalysts for diesel soot emissions control: an overview. Catal. Rev. **56**, 57–81 (2014)
60. S. Bensaid, G.A. Blengini, D. Fino, N. Russo, Diesel soot combustion with perovskite catalysts. Chem. Eng. Commun. **201**, 1327–1339 (2014)
61. A. Civera, M. Pavese, G. Saracco, V. Specchia, Combustion synthesis of perovskite-type catalysts for natural gas combustion. Catal. Today **83**, 199–211 (2003)
62. M. Haneda, A. Towata, Catalytic performance of supported Ag nano-particles prepared by liquid phase chemical reduction for soot oxidation. Catal. Today **242**, 351–356 (2015)
63. A. Serve, A. Boreave, B. Cartoixa, K. Pajot, P. Vernoux, Synergy between Ag nanoparticles and yttria-stabilized zirconia for soot oxidation. Appl. Catal. B Environ. **242**, 140–149 (2019)
64. E. Obeid, L. Lizarraga, M.N. Tsampas, A. Cordier, A. Boréave, M.C. Steil, G. Blanchard, K. Pajot, P. Vernoux, Continuously regenerating diesel particulate filters based on ionically conducting ceramics. J. Catal. **309**, 87–96 (2014)
65. E. Obeid, M.N. Tsampas, S. Jonet, A. Boréave, L. Burel, M.C. Steil, G. Blanchard, K. Pajot, P. Vernoux, Isothermal catalytic oxidation of diesel soot on yttria-stabilized zirconia. Solid State Ionics **262**, 253–256 (2014)
66. L. Castoldi, E. Aneggi, R. Matarrese, R. Bonzi, A. Trovarelli, L. Lietti, Simultaneous removal of soot and NO_x over silver and ruthenium-based catalysts. Top. Catal. **60**, 209–213 (2017)
67. L. Dou, T. Fan, H. Zhang, A novel 3D oxide nanosheet array catalyst derived from hierarchical structured array-like CoMgAl-LDH/graphene nanohybrid for highly efficient NO_x capture and catalytic soot combustion. Catal. Sci. Technol. **5**, 5153–5167 (2015)
68. P. Legutko, T. Jakubek, W. Kaspera, P. Stelmachowski, Z. Sojka, A. Kotarba, Strong enhancement of desoot activity of transition metal oxides by alkali doping: additive effects of potassium and nitric oxide. Top. Catal. **60**, 162–170 (2017)
69. G. Mul, J.P.A. Neeft, F. Kapteijn, M. Makkee, J.A. Moulijn, Soot oxidation catalyzed by a Cu/K/Mo/Cl catalyst: evaluation of the chemistry and performance of the catalyst. Appl. Catal. B Environ. **6**, 339–352 (1995)
70. A. Carrascull, I.D. Lick, E.N. Ponzi, M.I. Ponzi, Catalytic combustion of soot with a O_2/NO mixture. KNO_3/ZrO_2 catalysts. Catal. Commun. **4**, 124–128 (2003)
71. L. Sui, L. Yu, Y. Zhang, Catalytic combustion of diesel soot on Co-Sr-K catalysts. Energy Fuel **21**, 1420–1424 (2007)
72. H. An, P.J. McGinn, Catalytic behavior of potassium containing compounds for diesel soot combustion. Appl. Catal. B Environ. **62**, 46–56 (2006)
73. D. Courcot, C. Pruvost, E.A. Zhilinskaya, A. Aboukaïs, Potential of supported copper and potassium oxide catalysts in the combustion of carbonaceous particles. Kinet. Catal. **45**, 580–588 (2004)
74. H. Laversin, D. Courcot, E.A. Zhilinskaya, R. Cousin, A. Aboukaïs, Study of active species of Cu-K/ZrO_2 catalysts involved in the oxidation of soot. J. Catal. **241**, 456–464 (2006)
75. N.F. Galdeano, A.L. Carrascull, M.I. Ponzi, I.D. Lick, E.N. Ponzi, Catalytic combustion of particulate matter: catalysts of alkaline nitrates supported on hydrous zirconium. Thermochim. Acta **421**, 117–121 (2004)

76. W. Kaspera, P. Indyka, Z. Sojka, A. Kotarba, Bridging the gap between tight and loose contacts for soot oxidation by vanadium doping of cryptomelane nanorods catalyst using NO_2 as an oxygen carrier. Catal. Sci. Technol. **8**, 3183–3192 (2018)
77. T. Jakubek, K. Ralphs, A. Kotarba, H. Manyar, Nanostructured potassium-manganese oxides decorated with Pd nanoparticles as efficient catalysts for low-temperature soot oxidation. Catal. Lett. **149**, 100–106 (2019)
78. H. Zhang, S. Yuan, J.L. Wang, M. Gong, Y. Chen, Effects of contact model and NO_x on soot oxidation activity over Pt/MnO_x-CeO_2 and the reaction mechanisms. Chem. Eng. J. **327**, 1066–1076 (2017)
79. Q. Shen, G. Lu, C. Du, Y. Guo, Y. Wang, Y. Guo, X. Gong, Role and reduction of NO_x in the catalytic combustion of soot over iron-ceria mixed oxide catalyst. Chem. Eng. J. **218**, 164–172 (2013)
80. J.M. Christensen, J.D. Grunwaldt, A.D. Jensen, Effect of NO_2 and water on the catalytic oxidation of soot. Appl. Catal. B Environ. **205**, 182–188 (2017)
81. N. Zouaoui, M. Issa, D. Kehrli, M. Jeguirim, CeO_2 catalytic activity for soot oxidation under NO/O_2 in loose and tight contact. Catal. Today **189**, 65–69 (2012)
82. P. Miceli, S. Bensaid, N. Russo, D. Fino, CeO_2-based catalysts with engineered morphologies for soot oxidation to enhance soot-catalyst contact. Nanoscale Res. Lett. **9**, 254 (2014)
83. E. Aneggi, C. de Leitenburg, A. Trovarelli, On the role of lattice/surface oxygen in ceria-zirconia catalysts for diesel soot combustion. Catal. Today **181**, 108–115 (2012)
84. E. Aneggi, C. de Leitenburg, J. Llorca, A. Trovarelli, Higher activity of diesel soot oxidation over polycrystalline ceria and ceria-zirconia solid solutions from more reactive surface planes. Catal. Today **197**, 119–126 (2012)
85. P.A. Kumar, M.D. Tanwar, S. Bensaid, N. Russo, D. Fino, Soot combustion improvement in diesel particulate filters catalyzed with ceria nanofibers. Chem. Eng. J. **207–208**, 258–266 (2012)
86. S. Bensaid, N. Russo, D. Fino, CeO_2 catalysts with fibrous morphology for soot oxidation: the importance of the soot-catalyst contact conditions. Catal. Today **216**, 57–63 (2013)
87. P. Miceli, S. Bensaid, N. Russo, D. Fino, Effect of the morphological and surface properties of CeO_2-based catalysts on the soot oxidation activity. Chem. Eng. J. **278**, 190–198 (2015)
88. W. Zhang, X. Niu, L. Chen, F. Yuan, Y. Zhu, Soot combustion over nanostructured ceria with different morphologies. Sci. Rep. **6**, 29062 (2016)
89. M. Piumetti, S. Bensaid, N. Russo, D. Fino, Nanostructured ceria-based catalysts for soot combustion: investigations on the surface sensitivity. Appl. Catal. B Environ. **165**, 742–751 (2015)
90. E. Aneggi, D. Wiater, C. de Leitenburg, J. Llorca, A. Trovarelli, Shape-dependent activity of ceria in soot combustion. ACS Catal. **4**, 172–181 (2014)
91. Y. Cheng, J. Liu, Z. Zhao, Y. Wei, Y. Song, C. Xu, The simultaneous purification of PM and NO_x in diesel engine exhausts over a single 3DOM $Ce_{0.9-x}Fe_{0.1}Zr_xO_2$ catalyst. Environ. Sci. Nano **4**, 1168–1177 (2017)
92. K. Hinot, H. Burtscher, A.P. Weber, G. Kasper, The effect of the contact between platinum and soot particles on the catalytic oxidation of soot deposits on a diesel particle filter. Appl. Catal. B Environ. **71**, 271–278 (2007)
93. D. Fino, N. Russo, E. Cauda, G. Saracco, V. Specchia, La-Li-Cr perovskite catalysts for diesel particulate combustion. Catal. Today **114**, 31–39 (2006)
94. N. Russo, D. Fino, G. Saracco, V. Specchia, Promotion effect of Au on perovskite catalysts for the regeneration of diesel particulate filters. Catal. Today **137**, 306–311 (2008)
95. J. Caroca, G. Villata, D. Fino, N. Russo, Comparison of different diesel particulate filters. Top. Catal. **52**, 2076–2082 (2009)
96. L. Tang, Z. Zhao, K. Li, X. Yu, Y. Wei, J. Liu, Y. Peng, Y. Li, Y. Chen, Highly active monolith catalysts of $LaKCoO_3$ perovskite-type complex oxide on alumina-washcoated diesel particulate filter and the catalytic performances for the combustion of soot. Catal. Today **339**, 159–173 (2020)

97. Q. Zhou, K. Zhong, W. Fu, Q. Huang, Z. Wang, B. Nie, Nanostructured platinum catalyst coating on diesel particulate filter with a low-cost electroless deposition approach. Chem. Eng. J. **270**, 320–326 (2015)
98. V. Di Sarli, G. Landi, L. Lisi, A. Di Benedetto, Ceria-coated diesel particulate filters for continuous regeneration. AICHE J. **63**, 3442–3449 (2017)
99. V. Di Sarli, A. Di Benedetto, Modeling and simulation of soot combustion dynamics in a catalytic diesel particulate filter. Chem. Eng. Sci. **137**, 69–78 (2015)
100. V. Di Sarli, A. Di Benedetto, Operating map for regeneration of a catalytic diesel particulate filter. Ind. Eng. Chem. Res. **55**, 11052–11061 (2016)
101. V. Di Sarli, A. Di Benedetto, Combined effects of soot load and catalyst activity on the regeneration dynamics of catalytic diesel particulate filters. AICHE J. **64**, 1714–1722 (2018)
102. V. Di Sarli, A. Di Benedetto, Using CFD simulation as a tool to identify optimal operating conditions for regeneration of a catalytic diesel particulate filter. Appl. Sci. (Basel) **9**, 3453 (2019)
103. S. Wagloehner, M. Nitzer-Noski, S. Kureti, Oxidation of soot on manganese oxide catalysts. Chem. Eng. J. **259**, 492–504 (2015)
104. E. Bruneel, J. Van Brabant, M.T. Le, I. Van Driessche, Deposition of a Cu/Mo/Ce catalyst for diesel soot oxidation on a sintered metal fiber filter with a CeO_2 anti corrosion coating. Catal. Commun. **25**, 111–117 (2012)
105. S.A. Leonardi, F.E. Tuler, E.M. Gaigneaux, D.P. Debecker, E.E. Miró, V.G. Milt, Novel ceramic paper structures for diesel exhaust purification. Environ. Sci. Pollut. Res. **25**, 35276–35286 (2018)
106. N.A. Sacco, E.D. Banús, J.P. Bortolozzi, V.G. Milt, E.E. Miró, Ultrasound-assisted deposition of Co-CeO_2 onto ceramic microfibers to conform catalytic papers: their application in engine exhaust treatment. ACS Omega **3**, 18334–18342 (2018)